Chapter 5
Controlling Chaos

Chaotic dynamics is one of the most general ways of non-linear systems evolution. Chaotic regimes are abundantly present in nature as well as in devices created by human hands. However, it is difficult to unambiguously answer whether chaos is useful or harmful. Chaos is beneficial when it increases the chemical reaction rate by intensifying mixing, providing a powerful mechanism for heat and mass transfer. However, in many situations chaos is an undesirable phenomenon which can, for example, lead to additional mechanical fatigue of the elements of construction due to their irregular vibrations. The possibility of non-resonant energy absorption in a chaotic regime can lead the system parameters beyond safe levels. Therefore, it is clear that the ability to control chaos, i.e., to enforce or suppress it, has great practical importance. Earlier, when chaos was still unusual, the problem of its amplification was at the center of attention. However, at the beginning of the 1990s, the pendulum swung in the other direction. Considerable theoretical and experimental efforts were made to convert chaos into periodic motion. A new and intensely developing domain of non-linear dynamics—controlled chaos—originated from the pioneering work [1] of the same name. From this point on the term "controlled chaos" entered into the vocabulary of physicists which deal with non-linear dynamical systems.

5.1 Statement of the Problem

All of the numerous definitions of chaos are based on the extreme sensitivity of chaotic dynamics to initial conditions. In the real world any system is disturbed by external noise, and in computer simulations a small perturbation appears due to numerical round-off. If a system is chaotic, then a small perturbation grows exponentially in time, drastically changing the behavior of the system. This peculiarity of chaotic systems considerably complicates analysis, driving experimenters

Y. Bolotin et al., *Chaos: Concepts, Control and Constructive Use*,
Understanding Complex Systems, DOI 10.1007/978-3-319-42496-5_5

to despair. However, the reason for despair may become the origin of hope. After all, if the system is so sensitive to small perturbations, can we use them to control it? This idea is the basis for the Ott–Grebogy–Yorke (OGY) control method [1].

It is interesting to note that in the pioneering work [1] there was already a deep understanding of the prospective aim of chaos control. "One may want a system to be used for different purposes or under different conditions at different times. Thus, depending on the use, different requirements are made of the system. If the system is chaotic, this type of multiple-use situation might be accommodated without alteration of the gross system configuration. In contrast, in the absence of chaos, completely separate systems might be required for each use. Such multipurpose flexibility is essential to higher life forms, and we, therefore, speculate that chaos may be a necessary ingredient in their regulation by the brain."

The OGY method and its numerous variations are based on the fundamental concept of global reconstruction of the system due to small perturbation. They are used for chaos control both in abstract models and in different concrete systems beginning with the simplest pendulum [2] and ending with the such complex biological systems as the heart [3] and brain [4].

Practically any dynamical system can be an object for control. At the present time the best results are achieved in the domain of control for systems with dynamics which are chaotic over time. They are described by systems of ordinary differential equations and are finite-dimensional inherently. The dynamics of such a system can also be described using mappings in terms of discrete time. Such transitions can be performed using the well-known technique of Poincaré sections (see Sect. 3.1). Systems with spatially chaotic dynamics are also described by systems of ordinary differential equations. The realization of control in such systems requires only minor modification of the methods used for systems chaotic in time. Infinite-dimensional systems with dynamics which are chaotic both in time and in space are described by equations in partial derivatives. It is the control of such systems that now presents the main difficulty, though even in this domain considerable progress has been achieved.

One of the most attractive features of the developed control methods is that it is not necessary to have any analytical model of the controlled system. For input information describing the system dynamics we can use masses of experimental data of any dimension. This feature of the control methods opens up the possibility for its application to practically any system if its dynamics contain a chaotic component.

5.2 Discrete Parametric Control and Its Strategy

In any chaos control method the principal role is played by the immediate objects of stabilization, which are the unstable periodic orbits. One of the fundamental properties of chaos is the simultaneous coexistence of many different motions in the system. In particular, chaotic motion on the strange attractor coexists with an infinite number of unstable periodic orbits. The motion of the system along a chaotic orbit can be understood as the continuous switching between neighboring unstable

periodic orbits [5]. One can imagine the periodic orbits as forming the skeleton of the chaotic attractor, supporting dynamics in the phase space. The same fundamental role is played by periodic orbits in quantum mechanics as well. We will cite just the famous trace formula [6], which allows the quantum spectrum to be linked in semiclassical approach with a sum over classical periodic orbits.

Although the existence of unstable periodic orbits does not apparently manifest in free chaotic evolution, these objects play a principal role from the point of view of chaos control. In order to demonstrate this, we shall discuss the strategy first realized in the OGY chaos control method. Let us consider a set of unstable periodic orbits embedded in the chaotic attractor of a dynamical system. For each of such orbits we shall ask the question: does motion on that trajectory optimize some system characteristic? Then we choose one of the optimal trajectories. Assuming that motion on the attractor is ergodic, we can always wait until the moment of time when the chaotic trajectory during its random walks approaches the chosen unstable periodic orbit. When it happens, we apply a small programmed perturbation in order to direct the trajectory towards the target orbit. If there is noise present in the system, we shall repeat that procedure in order to keep the periodic orbit.

To realize that strategy we need to do the following:

- to identify the unstable periodic orbits on the attractor;
- to study the attractor structure in the neighborhood of such orbits;
- to choose the system parameters appropriate for realization of control and to study the system response on their perturbation.

Perhaps the most difficult step in this strategy is the localization of the unstable periodic orbits. A whole row of papers [7–10] is devoted to this problem. However, the method which is the most closely related with the main idea of chaos control is the one based on the transformation of unstable objects into stable ones [11]. The essence of the method is in utilizing the universal set of linear transformations, which allow the transformation of unstable periodic orbits into the stable ones, localized in the same points of the phase space as the required unstable orbits. Stable periodic orbits obtained as the result of such transformation can be found with the help of standard iterative procedures. Analysis of the attractor structure in the neighborhood of unstable fixed points or unstable periodic orbits (which can be considered as the combinations of unstable fixed points) does not present any problem. To do this, one should observe the motion of the point representing the current state of the system in the Poincaré section surface. From time to time this point will approach the unstable fixed point along the direction which is called the stable one, and then it will move off along the unstable direction. These two directions form a geometric structure which is called the saddle. Knowledge of those directions (the eigenvectors of the Jacobi matrix) and the velocities of approaching and moving off along those directions (the eigenvalues of the Jacobi matrix) represent all the necessary information about the local structure of the attractor in the neighborhood of the fixed point, which is needed for the realization of the discrete parametric control method.

The identification of optimal system parameters is a relatively difficult task. We note that a number of modifications of the OGY method [12] permit this difficulty to be avoided. But as soon as the choice is made, there remains only to determine the positions of the unstable periodic orbits for a few parameter values close to the nominal one. This is all the necessary information needed for the realization of the discrete parametric control of chaos by the OGY method.

For a better understanding of the fundamental ideas lying at the core of this method, disregarding the difficulties connected with multidimensionality, let us perform chaos control [13] in one-dimensional logistic mapping

$$X_{n+1} = f(X_n, p) = pX_n(1 - X_n)\,, \tag{5.1}$$

where X is limited in the interval $[0, 1]$, and p is the unique parameter of the mapping. It is well known [14] that one of the mechanisms of transition to chaos in that mapping is period doubling. As p grows, a sequence of period doubling bifurcations takes place at which the orbits with consecutive period doubling became stable. Period doubling bifurcations cascade ends at $p = p_\infty \approx 3.57$, after which chaos begins.

Let us assume that we want to avoid chaos at $p = 3.8$. More specifically, we want the trajectory with randomly chosen initial conditions to be as close as possible to some unstable periodic orbit, assuming that this orbit optimizes some system characteristic. Thus we will consider that we can only fine tune p near the value $p_0 = 3.8$, i.e., let us limit the range of variation for the parameter p by the interval $(p_0 - \delta, p_0 + \delta;\ \delta \ll 1)$.

In view of the fact that the motion is ergodic, a trajectory with arbitrary initial condition X_0 with unit probability will sooner or later appear in a neighborhood of the chosen periodic orbit. However, because of its chaotic nature (exponential divergence) the trajectory will quickly deviate from the periodic orbit. Our task is to program the parameter variation so that the trajectory will stay in the neighborhood of the periodic orbit during the control time. We stress that according to the very formulation of the problem we can use only a small perturbation of the parameter. Otherwise, chaos itself can be excluded, for example, changing the parameter p from 3.8 to 2.

Let us consider the orbit with period i:

$$X_0(1) \to X_0(2) \to \cdots X_0(i) \to X_0(i + 1) = X_0(1)\,.$$

If in the moment of time n the chaotic trajectory appeared in the neighborhood of the mth component of the periodic orbit, then the linearized dynamics in the

neighborhood of that component reads as the following:

$$X_{n+1} - X_0(m+1) = \left.\frac{\partial f(X,p)}{\partial X}\right|_{X=X_0(m),p=p_0} \delta X_n + \left.\frac{\partial f(X,p)}{\partial p}\right|_{X=X_0(m),p=p_0} \delta p_n = p_0[1-2X_0(m)]\delta X_n + X_0(m)[1-X_0(m)]\delta p_n\,,$$

here $\delta X_n \equiv X_n - X_0(m)$, $\delta p_n = p_n - p_0$. Requiring that $X_{n+1} = X_0(m+1)$, we obtain the parameter perturbation, needed for $n+1$ iteration to get on the periodic orbit

$$\delta p_n = p_0 \frac{[2X_0(m)-1]\,\delta X_n}{X_0(m)\,[1-X_0(m)]}\,. \tag{5.2}$$

Relation (5.2) takes place if only the trajectory X_n appears in a small neighborhood of the chosen periodic orbit, i.e., when $\delta X_n \ll 1$ and, therefore, the perturbation δp_n is small. Otherwise the system evolves according to the initial parameter value p_0.

The procedure described above is convenient because it allows us to stabilize different periodic orbits in different times. Let us assume that we stabilized a chaotic trajectory in the neighborhood of some periodic orbit, for example, one of period 2. Then we decided to stabilize the period-1 orbit, i.e., an unstable fixed point, assuming that it is the orbit that optimizes some system characteristic in the present time. Let us switch off the control. After that, the trajectory starts to deviate exponentially quickly from the period-2 orbit. Due to ergodicity, after some time the trajectory will appear in the small neighborhood of the chosen fixed point. In that moment of time, we shall switch on the control, but for the unstable fixed point [calculated according to (5.2)], and we will stabilize the chaotic trajectory in its neighborhood. The result is described in Fig. 5.1a.

In the presence of external noise the controlled trajectory can be accidentally kicked out from the periodic orbit neighborhood. If this happens, we should switch off the control and let the system evolve freely until the chaotic trajectory returns to the neighborhood of the target periodic orbit, and the control can be resumed within the given range of parameter variation. For additive Gaussian noise it is easy to check that the average length of the controlled phase grows with the decreasing of noise amplitude. This situation is illustrated in Fig. 5.1b. The noise is modeled by additive term in the logistic mapping of the form $\eta\sigma$, where η is the noise amplitude, and σ is the Gaussian distributed random variable with zero average value and unit dispersion.

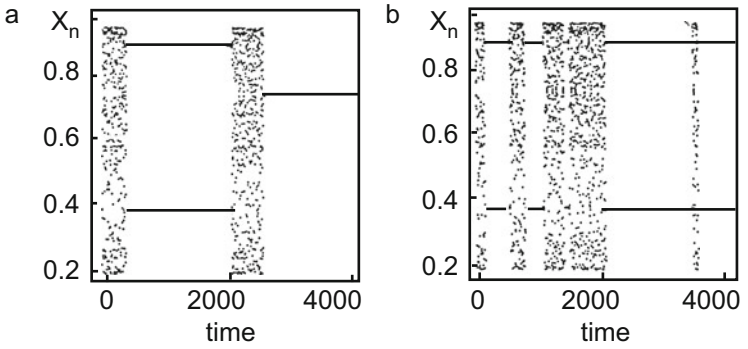

Fig. 5.1 (**a**) Control of unstable periodic orbit with period 2 in the logistic mapping in absence of noise; (**b**) control of the same orbit in presence of additive Gaussian noise $\left(\eta = 2.6 \times 10^{-4}\right)$ [13]

5.3 Main Equations for Chaos Control

Having illustrated the general strategy of the parametric control in the one-dimensional example, we now turn to multidimensional system control. For simplicity, we will consider the case of control for an unstable fixed point in two-dimensional phase space. This example contains all the basic features of multidimensionality.

We consider a three-dimensional continuous system with a two-dimensional Poincaré section, dynamics of which are described by the following mapping:

$$\mathbf{Z}_{n+1} = \mathbf{F}\left(\mathbf{Z}_n, p\right) , \tag{5.3}$$

where p is some parameter tunable in a small interval $\delta \ll 1$,

$$|p - p_0| < \delta , \tag{5.4}$$

around some initial value p_0.

The key difference between one-dimensional and two-dimensional (multidimensional) cases is the fact that in the latter, any unstable fixed point is connected with some geometrical structure, namely for each fixed point (or for every component of periodic orbit) there exist stable and unstable directions, which we mentioned before. The control strategy, accounting for the complication of geometry, consists of the following. Any time when the point $\mathbf{Z}_n$ of intersection of the orbit with the Poincaré section surface appears sufficiently close to the fixed point $\mathbf{Z}_F(p_0) = \mathbf{F}(\mathbf{Z}_F(p_0), p_0)$, the controlling parameter p acquires the new value p_n, such that after consecutive iteration, the point $\mathbf{Z}_{n+1} = \mathbf{F}(\mathbf{Z}_n, p_n)$ gets on the local stable manifold of the fixed point $\mathbf{Z}_F(p_n)$.

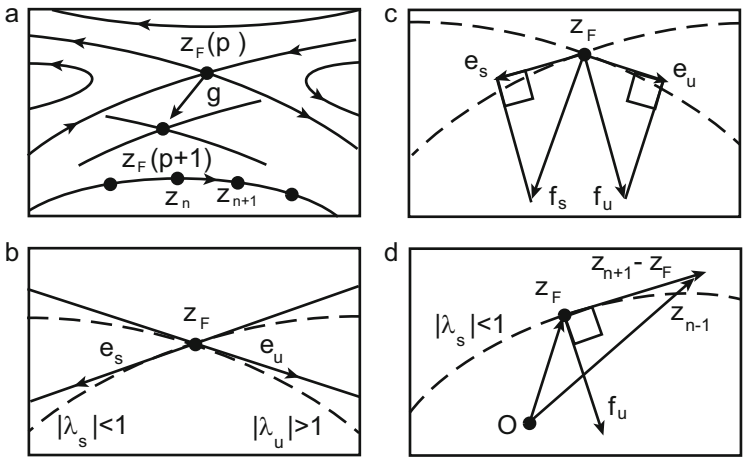

Fig. 5.2 (**a**) Shift of the unstable fixed point with variation of the parameters; (**b**) eigenvectors of the Jacobi matrix $(\mathbf{e}_u, \mathbf{e}_s)$ for the fixed point $\mathbf{Z}_F$; (**c**) auxiliary basis $(\mathbf{f}_u, \mathbf{f}_s)$; (**d**) iteration of the mapping in the neighborhood of the fixed point necessary to realize the control [15]

Let us realize this strategy [1, 15]. Shift of the fixed point due to variation of the parameter $(p_0 \to p_n = p_0 + \delta p_n)$ equals

$$\mathbf{Z}_F(p_n) = \mathbf{Z}_F(p_0) + \mathbf{g}\,\delta p_n\,, \tag{5.5}$$

where the shift vector of the fixed point is $\mathbf{g} = \left.\frac{d\mathbf{Z}_F(p)}{dp}\right|_{p=p_0}$ (see Fig. 5.2a).

Linearized dynamics in the neighborhood of the fixed point $\mathbf{Z}_F(p_0)$ looks like the following:

$$\mathbf{Z}_{n+1} - \mathbf{Z}_F(p_n) \cong \hat{A}(p_0)\,(\mathbf{Z}_n - \mathbf{Z}_F(p_n))\,, \tag{5.6}$$

where $A_{ij} = \left.\frac{\partial F_i}{\partial Z_j}\right|_{\mathbf{Z}=\mathbf{Z}_F(p_0),p=p_0}$ is the Jacobi matrix.

The Jacobi matrix $\hat{A}$ is characterized by its eigenvectors $\mathbf{e}_u, \mathbf{e}_s$ and eigenvalues λ_u, λ_s,

$$\hat{A}\mathbf{e}_u = \lambda_u \mathbf{e}_u$$
$$\hat{A}\mathbf{e}_s = \lambda_s \mathbf{e}_s\,,$$

where the indices u and s correspond, respectively, to unstable and stable directions of $\mathbf{Z}_F(p_0)$ (see Fig. 5.2b): $|\lambda_s| < 1 < |\lambda_u|$. These eigenvectors are normalized, but they are not orthogonal:

$$\mathbf{e}_s^T\mathbf{e}_s = \mathbf{e}_u^T\mathbf{e}_u = 1, \quad \mathbf{e}_s^T\mathbf{e}_u \neq 0\,, \tag{5.7}$$

where the symbol T denotes the transposition operation. The Jacobi matrix can be presented in the form:

$$\hat{A} = [\mathbf{e}_u \mathbf{e}_s] \begin{pmatrix} \lambda_u & 0 \\ 0 & \lambda_s \end{pmatrix} [\mathbf{e}_u \mathbf{e}_s]^{-1} .$$

Because of non-orthogonality of the vectors $\mathbf{e}_u$ and $\mathbf{e}_s$ it is convenient for formulation of the control to introduce a new "orthogonal" basis $\{\mathbf{f}_u, \mathbf{f}_s\}$ (see Fig. 5.2c):

$$\mathbf{f}_s^T \mathbf{e}_s = \mathbf{f}_u^T \mathbf{e}_u = 1; \quad \mathbf{f}_u^T \mathbf{e}_s = \mathbf{f}_s^T \mathbf{e}_u = 0 . \tag{5.8}$$

Those are connected to bases by the simple relation

$$\begin{pmatrix} f_{u1} & f_{u2} \\ f_{s1} & f_{s2} \end{pmatrix} = \begin{pmatrix} e_{u1} & e_{s1} \\ e_{u2} & e_{s2} \end{pmatrix}^{-1} .$$

From the latter we obtain components for the new basis:

$$\begin{aligned} f_{u1} &= e_{s2}/\Delta, \quad f_{u2} = -e_{s1}/\Delta, \\ f_{s1} &= -e_{u2}/\Delta, \quad f_{s2} = e_{u1}/\Delta; \\ \Delta &\equiv e_{u1} e_{s2} - e_{s1} e_{u2} . \end{aligned}$$

The Jacobi matrix can be expressed also in the mixed e,f-basis:

$$\hat{A} = \lambda_u \mathbf{e}_u \cdot \mathbf{f}_u^T + \lambda_s \mathbf{e}_s \mathbf{f}_s^T .$$

Projecting this relation on the direction $\mathbf{f}_u$, we obtain a useful result

$$\mathbf{f}_u^T \hat{A} = \lambda_u \mathbf{f}_u^T . \tag{5.9}$$

We can now formulate the control condition—getting $\mathbf{Z}_{n+1}$ on the local stable manifold (see Fig. 5.2d) $\mathbf{Z}_F(p_0)$—in the following form:

$$\mathbf{f}_u^T \delta \mathbf{Z}_{n+1} = 0; \quad \delta \mathbf{Z}_{n+1} = \mathbf{Z}_{n+1} - \mathbf{Z}_F(p_0) . \tag{5.10}$$

Substituting (5.5) into (5.6) and using (5.9) together with the control condition (5.10), we get the following:

$$\delta p_n = \frac{\lambda_u}{\lambda_u - 1} \frac{\mathbf{f}_u^T \delta \mathbf{Z}_n}{\mathbf{f}_u^T \mathbf{g}} . \tag{5.11}$$

Relation (5.11) is the basic formula of the discrete parametric OGY control.

This result can also be represented in an alternative form. Simultaneously accounting the transition $\mathbf{Z}_n \to \mathbf{Z}_{n+1}$ and variation of the parameter $p_0 \to p_0 + \delta p_n$, we can present the dynamics in the neighborhood of the fixed point $\mathbf{Z}_F(p_0)$ in the following form:

$$\delta \mathbf{Z}_{n+1} \simeq \hat{A}(p_0)\delta \mathbf{Z}_n + \mathbf{B}\delta p_n; \quad \mathbf{B} = \left.\frac{\partial \mathbf{F}}{\partial p}\right|_{\mathbf{Z}=\mathbf{Z}_F(p_0),p=p_0}. \tag{5.12}$$

Projecting (5.12) on the direction $\mathbf{f}_u$ and utilizing the control condition (5.10), we get

$$\delta p_n = -\lambda_u \frac{\mathbf{f}_u^T \delta \mathbf{Z}_n}{\mathbf{f}_u^T \mathbf{B}}. \tag{5.13}$$

Vectors $\mathbf{B}$ and $\mathbf{g}$ are connected with the relation

$$\mathbf{B} = \left(1 - \hat{A}\right)\mathbf{g}.$$

The main result of the OGY control method can be presented in the form

$$\delta p_n = C\mathbf{f}_u^T \delta \mathbf{Z}_n, \tag{5.14}$$

which we can interpret in the following way. Deviation of the parameter from its initial value δp_n, necessary to perform the control, is proportional to the projection of the vector $\delta \mathbf{Z}_n$ onto the stable direction $\mathbf{f}_u$. The proportionality coefficient C is calculated from the fixed point shift $\mathbf{g}$ projection onto the same direction and from the unstable eigenvalue λ_u.

Let us now turn to the geometrical interpretation of the obtained result. Figure 5.3 represents the point $\mathbf{Z}_n$, approaching the unstable fixed point $Z_F(p_0)$ along the stable direction $\mathbf{e}_s$. In absence of control in the consecutive moments of time, the point will move off the $Z_F(p_0)$ along the unstable direction $\mathbf{e}_u$. Let us now introduce into the system such parameter perturbation δp_n, that the point $\mathbf{Z}_n$, determining the system position, will appear to lie between the new and old stable directions (Fig. 5.3b). Motion along the new stable direction $\mathbf{e}_s'$ with consecutive moving off the new unstable fixed point $\mathbf{Z}_F(p_0 + \delta p_n)$ along the unstable direction $\mathbf{e}_u'$ will be at the same time a motion towards the old stable fixed point $\mathbf{Z}_F(p_0)$. Therefore, if we properly choose δp_n [according to the OGY formula (5.11)], we can then make it so that the point $\mathbf{Z}_{n+1}$ will get precisely onto the stable manifold $\mathbf{Z}_F(p_0)$. After that we return the parameter to its initial value p_0, and the point describing the system position, remaining on the stable manifold, will approach $\mathbf{Z}_F(p_0)$ (Fig. 5.3c). A schematic three-dimensional analogue of the two-dimensional geometry of the OGY control is presented in Fig. 5.3d.

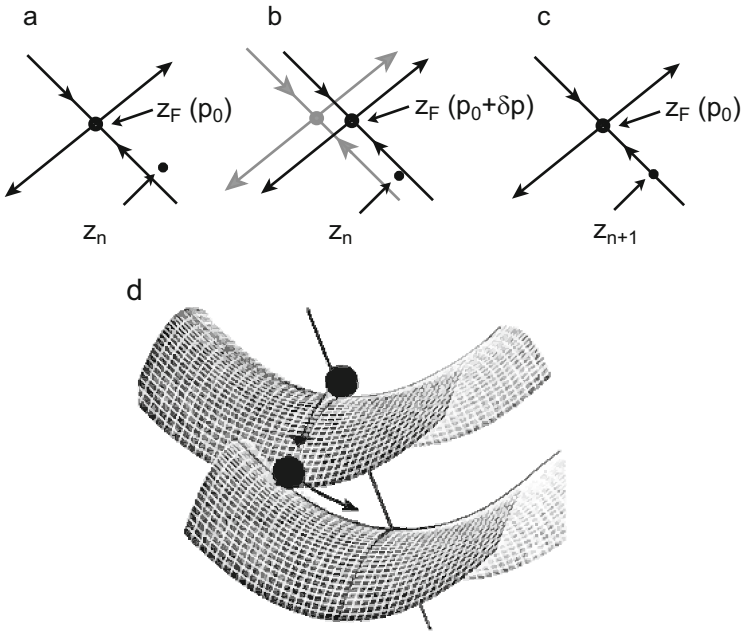

Fig. 5.3 (**a**) Point $\mathbf{Z}_n$ in the neighborhood of unstable fixed point Z_F (p_0); (**b**) shift of the fixed point with variation of the parameter $p_0 \to p_0 + \delta p_0$; (**c**) final stage of the OGY control; (**d**) schematic three-dimensional analogue of two-dimensional control geometry [1, 16]

As an example we consider the result of stabilization for the period-1 orbit in the Hénon mapping [17]

$$X_{n+1} = p - X_n^2 + 0.3Y_n$$
$$Y_{n+1} = X_n\,. \tag{5.15}$$

Starting from some randomly chosen initial condition on the attractor, the image point undergoes chaotic walks until at $n \sim 75$ it appears in the given neighborhood of the chosen unstable fixed point (it is marked by a cross in Fig. 5.4a). In that moment we turn on the control algorithm. The result of the control is presented in Fig. 5.4b. Figure 5.4c shows deviations of the parameter p from its nominal value ($p_0 = 1$), necessary to realize the control. In the absence of noise, the parameter deviations are non-zero only on the initial stage of control. Figure 5.4c presents deviation of the orbit δr_n from the unstable fixed point in logarithmic scale. After the control is turned off at ($n \sim 150$) the chaotic motion restores sufficiently quickly.

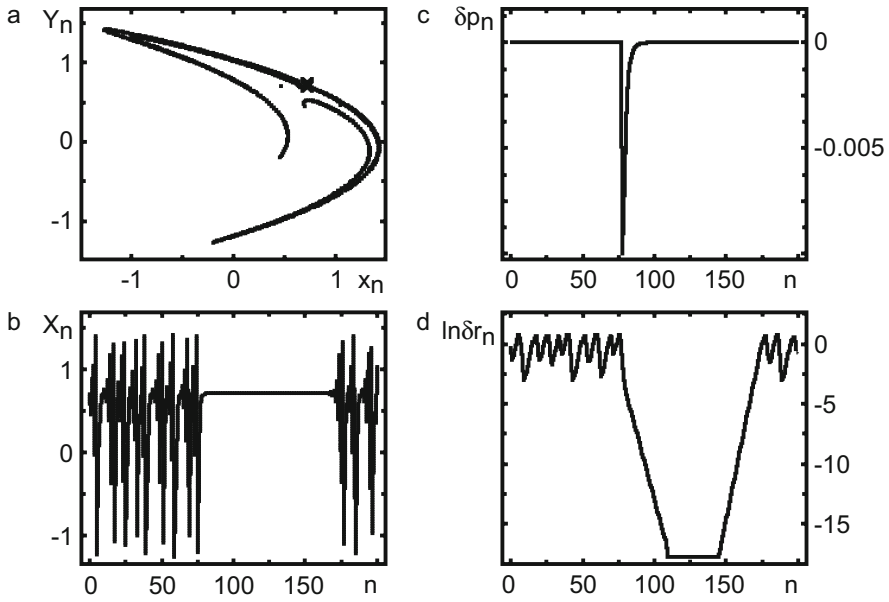

Fig. 5.4 OGY control for the Hénon mapping (without noise)

A logarithmic scale used in Fig. 5.4c sharply marks out all the characteristic stages of the control procedure:

1. chaotic motion up to the control turning on,
2. exponentially fast approach of the controlled trajectory to the unstable fixed point,
3. keeping in the neighborhood of the unstable fixed point with accuracy determined by numerical calculation errors,
4. exponential divergence of trajectories after the control is turned off,
5. restitution of free chaotic motion.

Let us consider in the same example the influence of noise on the described control mechanism. For that purpose, we add in the right-hand sides of the Hénon mapping (5.15) the terms $\varepsilon\delta X_n$ and $\varepsilon\delta Y_n$. Independent random variables δX_n and δY_n are Gaussian-distributed with zero mean values and unit dispersion. Figure 5.5 presents the result of stabilization for the unstable fixed point of the Hénon mapping for $\varepsilon = 0.014$. Even with the presence of noise, the OGY algorithm realizes the stabilization, but with a shortened control interval. In that case, the quantity δp_n is non-zero for whole duration of the control.

In conclusion, let us formulate the main advantages of the OGY discrete parametric control method:

The method requires minimum computational effort.

Realization of the control needs only small variations of the system parameters.

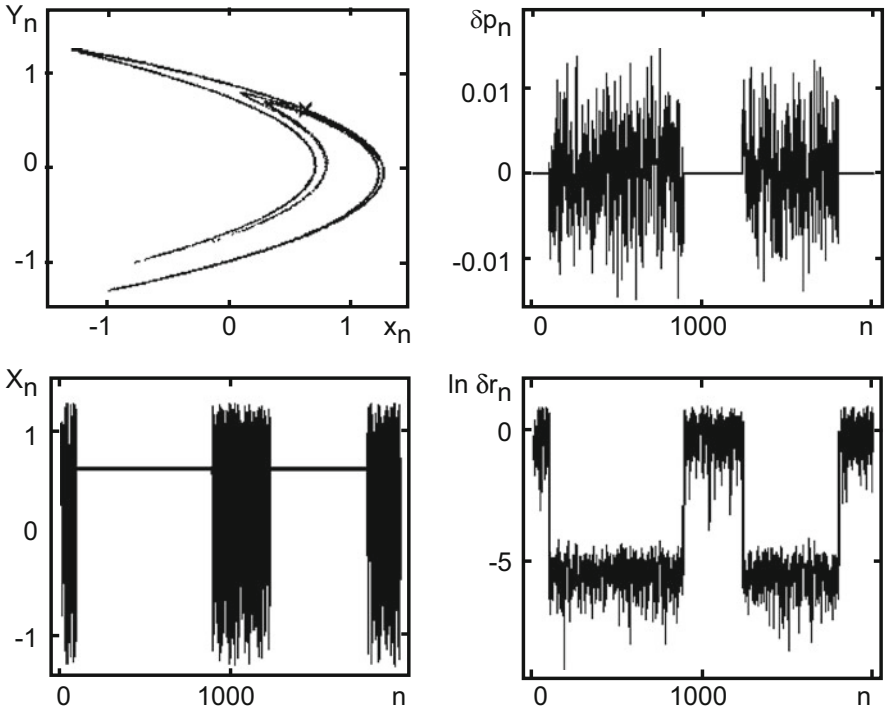

Fig. 5.5 OGY control for the Hénon mapping (with noise)

The control does not change the structure of the unperturbed system phase space.

Different unstable periodic orbits can be stabilized in common region of the parameter space.

The method can be applied to any non-linear system if its evolution allows description in terms of mappings.

The method does not require a priori model description of the dynamics. (The latter remark requires an explanation which will be given in the next section.)

5.4 Control of Chaos Without Motion Equations

The OGY method is based on a chaos control strategy that does not require a priori knowledge of equations of motion for the controlled object. As we have seen, realization of the method only requires knowledge of the local structure of the phase space in neighborhood of the target periodic orbit (or fixed point), i.e., the Jacobi matrix $\hat{A}$ and vector $\mathbf{g}(\mathbf{B})$, which enter into the relation (5.11) and (5.13). It can be shown [1, 18–20] that quantities can be reconstructed without an exact model (or equations of motion) of the controlled system.

This feature makes the OGY method particularly attractive for chaos control in real experiments. Indeed, with rare exceptions, experimentors do not have adequate models of the phenomena under investigation. To begin with, we will make an optimistic assumption that we know a sufficiently long segment of the dynamical system trajectory on the attractor (further on, we will weaken this assumption) and then we show how to reconstruct the information that interests us. Let the trajectory be given in the form of sufficiently long series of intersections $\mathbf{Z}_1, \mathbf{Z}_2 \ldots \mathbf{Z}_n$ with the Poincaré section surface. If two consecutive intersections, for example, $\mathbf{Z}_i$ and $\mathbf{Z}_{i+1}$, appear sufficiently close to each other ($(\mathbf{Z}_{i+1} - \mathbf{Z}_i)^2 \ll l^2$, where l is the characteristic size of the region of finite motion), then, generally speaking, the fixed point must be somewhere nearby. Having fixed the first pair, we will discover other analogous pairs in small neighborhood of the first "almost return." Because of ergodicity of motion on the strange attractor, there will be relatively many such pairs, if the trajectory is known for a sufficiently long time interval. We can try to reproduce the sequence of intersections with the help of linear mapping:

$$\mathbf{Z}_{n+1} = \hat{A}\mathbf{Z}_n + \mathbf{C}\,. \tag{5.16}$$

As noise is always present in the record of a real trajectory, in order to reproduce the matrix $\hat{A}$ and vector $\mathbf{C}$ we should use as many pairs as possible, adjusting the data with the method of least squares. Matrix $\hat{A}$, thus obtained, serves as an approximation of the Jacobi matrix, eigenvectors, and eigenvalues of which are required for the OGY control realization. The corresponding fixed point is approximated by the relation

$$\mathbf{Z}_F = (1 - \hat{A})^{-1}\mathbf{C}\,. \tag{5.17}$$

In order to find the approximate expression for the vector $\mathbf{g}$ one should change the parameter $p \to p + \Delta p$, reproduce the time series (trajectory) with that new value, redefine the fixed point $\mathbf{Z}_F(p + \Delta p)$, and find $\mathbf{g}$ as

$$\mathbf{g} = \frac{\mathbf{Z}_F(p + \Delta p) - \mathbf{Z}_F(p)}{\Delta p}\,. \tag{5.18}$$

To determine the quantities necessary for the stabilization of the period-2 orbit, one should perform an analogous procedure, but for closely intersecting pairs $\mathbf{Z}_n$ and $\mathbf{Z}_{n+2}$, and likewise for higher period orbits.

Let us illustrate the above-described procedure in the example of a non-linear pendulum subject to simplest periodic perturbation [2]. The non-linear pendulum, which for centuries represented the paradigm of periodic motion, is now often used to demonstrate the features of chaotic dynamics. The equation of motion for this system reads

$$\frac{d^2\theta}{dt^2} + k\frac{d\theta}{dt} + \sin\theta = f\cos\Omega t\,, \tag{5.19}$$

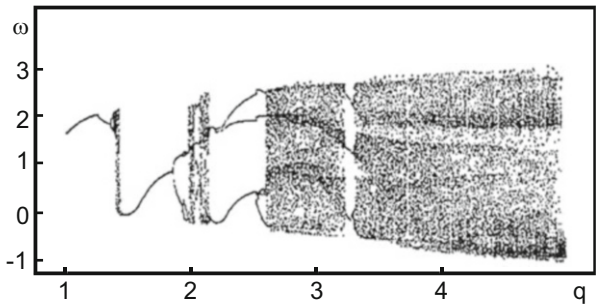

Fig. 5.6 Bifurcation diagram for forced oscillations of a non-linear pendulum [2]

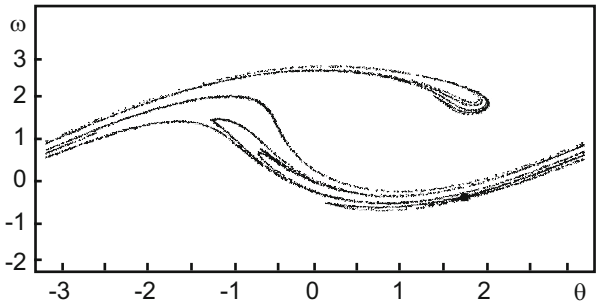

Fig. 5.7 Stroboscopic section for the non-linear pendulum; the *dark square* marks the unstable fixed point [2]

where θ is the angle of deviation from the vertical line, k is the friction coefficient, f and Ω are, respectively, the amplitude and the frequency of the driving force. Depending on the parameter values (k, f, Ω) the pendulum demonstrates different types of dynamical behavior. The bifurcation diagram (Fig. 5.6), which shows the angular velocity $\omega = d\theta/dt$ as a function of the parameter $q = 1/k$, reflects the graduate transition to chaos as the friction coefficient decreases. Further on, we will use the parameters set $(q = 3.9, f = 1.5, \Omega = 2/3)$, at which the pendulum dynamic is chaotic.

For now, let us assume that the equation of motion for the pendulum is unknown to us, but, observing the system experimentally, we can determine the quantities (θ_n, ω_n) in some discrete moments of time $t_n = nT$ $(T = 2\pi/\Omega)$. Laying these points on a plane (θ, ω), we get the so-called stroboscopic section—an analogue of the Poincaré section. This section is presented in Fig. 5.7. For the realization of the OGY control we must extract from the stroboscopic section the following information: the coordinates of the unstable fixed point (θ_F, ω_F); the dependence of the position of that point on the controlling parameter (if that parameter is $-q$), $(\partial\theta_F/\partial q,\ \partial\omega_F/\partial q)$; the Jacobi matrix in the neighborhood of the fixed point, its eigenvectors **e** and eigenvalues λ, the orthogonal basis **f**. Using the relations (5.16) and (5.17) for the set of points in the neighborhood $(1.5, 0.4)$ (the dark square on

Fig. 5.7), we find for the fixed point that

$$Z_F = \begin{pmatrix} \theta_F \\ \omega_F \end{pmatrix} = \begin{pmatrix} 1.523 \\ -0.415 \end{pmatrix}$$

and for the Jacobi matrix

$$\hat{A} = \begin{pmatrix} -3.42 & -5.79 \\ -1.52 & -2.48 \end{pmatrix}.$$

Eigenvalues and normalized eigenvectors for that matrix read

$$\lambda_u = -5.85, \quad \mathbf{e}_u = (e_{u1}, e_{u2}) = (0.92, 0.40)\,,$$
$$\lambda_s = +0.050, \quad \mathbf{e}_s = (e_{s1}, e_{s2}) = (0.86, -0.52)\,.$$

Using the relations (5.8) we can also find the orthogonal basis components necessary for control realization,

$$\mathbf{f}_u = (f_{u1}, f_{u2}) = (0.63, 1.04)\,,$$
$$\mathbf{f}_s = (f_{s1}, f_{s2}) = (0.49, -1.12)\,.$$

At last, we can determine how the variation of the friction coefficient affects the position of the fixed point. For small changes of the parameter q

$$\begin{pmatrix} \theta'_F \\ \omega'_F \end{pmatrix} \approx \begin{pmatrix} \theta_F \\ \omega_F \end{pmatrix} + \delta q \begin{pmatrix} \frac{\partial \theta_F}{\partial q} \\ \frac{\partial \omega_F}{\partial q} \end{pmatrix} = \mathbf{Z}_F + \mathbf{g}\delta q\,.$$

To determine vector $\mathbf{g}$ we shall follow the variation of the fixed point position with changes of parameter q. Having constructed the graphical dependencies $\theta(q)$ and $\omega(q)$, we can determine the components of the vector $\mathbf{g}$. We should note that the OGY control mechanism is not very sensitive to that parameter, therefore, in order to determine the vector $\mathbf{g}$ we can restrict ourself with a small number of dimensions. Now we have all the components necessary for the realization of the OGY control with the help of relation (5.11).

We should stress that we got all the necessary information only from the experimentally observable quantities $\theta(t)$, $\omega(t)$. The result of control for the period-1 unstable orbit (fixed point) is presented in Fig. 5.8. The control was turned on in the vicinity of the 1000th period of the external perturbation and was turned off near the 3000th period. About ten cycles were required to get the control. Only small variations of the controlling parameter $|\delta q| < 0.1$ were allowed during the control process. Large parameter changes could transfer the system into another dynamical regime (see the bifurcation diagram in Fig. 5.6). As we can see, during the control

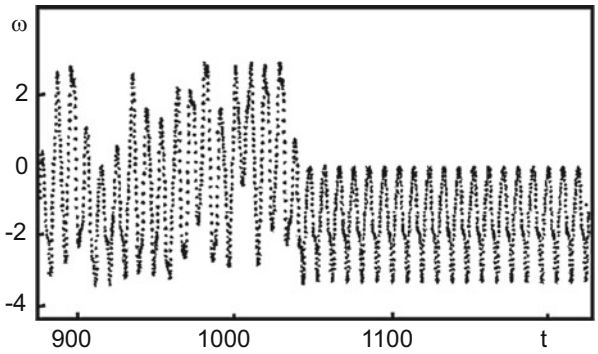

Fig. 5.8 Control of unstable fixed point for non-linear pendulum [2]

time, we were able to keep the chaotic trajectory in the vicinity of the target periodic orbit.

We should, however, note that it is difficult to measure experimentally the full N-dimensional vector of the system state in a given moment of time, but it is exactly this information which is required for the above procedure. As a limiting case, consider the situation where only one scalar system characteristic $f(t)$ is available for measurement. As Chap. 4 showed, it is possible to reconstruct the full dynamics of N-dimensional system from a single scalar characteristic.

5.5 Targeting Procedure in Dissipative Systems

In the control scheme considered above, with a limited interval of the controlling parameter variation ($|p_n - p_0| \leqslant \delta$) the control is turned on only after the trajectory being stabilized gets into ε-neighborhood ($\varepsilon \sim \delta$) of some component of the target periodic orbit. The efficiency of this control scheme is determined to a great extent by the time it takes to get into the required region or, as we shall say, control setup time.

Average time $\langle\tau\rangle$ required to get in the ε-vicinity of some point during chaotic motion on the strange attractor [1]

$$\langle\tau\rangle \sim \varepsilon^{-D}, \tag{5.20}$$

where D is the fractal dimension of the attractor (see [21, 22]). Therefore, if we do not make special efforts, the decrease of the allowed region of parameter variation will result in power-law growth of the control setup time. However, right after the appearance of the OGY control method, a procedure was proposed [23, 24], named "targeting" by its authors, which by special small change of the controlling parameter permitted the transformation of the control setup time growth law from

the power one to the essentially slower law—a logarithmic one. The procedure uses the exponential sensitivity of the chaotic trajectory to the initial conditions.

Let us discuss the targeting procedure in the simplest setup, when the attractor dimension is close to one [23, 24]. Generalizations on cases of higher dimension can be found in [25]. Suppose we have a time-continuous dynamical system, described by the equations of motion $\dot{\mathbf{x}} = \mathbf{F}(\mathbf{x})$. According to the usual scheme with the help of Poincaré sections we transit from the continuous equations of motions to the time-discrete reversible mapping

$$\mathbf{Z}_{n+1} = \mathbf{F}(\mathbf{Z}_n, p)\,. \tag{5.21}$$

Let us remember that if the equations of motion are not given, the Poincaré section can be reconstructed from experimental data. Suppose we want, starting from the point $\mathbf{Z}_s$, to get a small vicinity (with linear dimensions ε_t) of the point $\mathbf{Z}_t$. From now on, we will call this point the target. As usual, we assume that the system parameter p is subject only to small tuning on each iteration step:

$$p_n = p_0 + \delta p_n; \quad -\delta < \delta p_n < \delta; \quad |\delta| << p_0\,.$$

On the first iteration we include a small variation of the parameter $-\delta_1 < \delta p_1 < \delta_1$. Iterating (5.21) with values of p from the interval $[p_0 - \delta_1, p_0 + \delta_1]$, we get some segment ξ, passing through the point $\mathbf{F}(\mathbf{Z}_s, p_0)$. Let us denote length of that segment as $\delta\xi$. After that, we return back to the initial value of the parameter p_0. As the system is chaotic, the segment length will exponentially grow with each consecutive iteration. At long last, say, after η_1 iterations, it will reach size of the system. Without restricting the generalization, we can consider the linear dimensions of the attractor to be of the order of one. Then

$$\eta_1 \sim \lambda_1^{-1} \ln \delta\xi^{-1}\,. \tag{5.22}$$

Here λ_1 is the positive Lyapunov exponent of the mapping F. Similarly, if we will iterate vicinity of the target ε_t back in time, we find that the number of iterations required for that region to stretch up to the attractor dimensions equals

$$\eta_2 \sim |\lambda_2|^{-1} \ln \varepsilon_t^{-1}\,, \tag{5.23}$$

where λ_2 is the negative Lyapunov exponent of the mapping $\mathbf{F}^{-1}$. As both objects (the segment and the target vicinity) are stretched up to the attractor dimensions, we can find their intersection point. Iterating it η_1 times back in time, we find the point on the segment $\delta\xi$, which after $\eta_1 + \eta_2$ iterations maps into the target vicinity with linear dimensions ε_t. The total time required for this is

$$\tau = \lambda_1^{-1} \ln \delta\xi^{-1} + |\lambda_2|^{-1} \ln \varepsilon_t^{-1}\,. \tag{5.24}$$

Setting $\delta\xi \sim \varepsilon_t$, we obtain

$$\tau \sim \ln \varepsilon_t^{-1} , \tag{5.25}$$

contrary to the power-law growth without the targeting procedure.

The logarithmic behavior of the control setup time was confirmed in the following numerical experiment [23]. The source and the target were randomly chosen on the attractor of the Hénon mapping of the following form:

$$X_{n+1} = p - X_n^2 + 0.3Y_n$$
$$Y_{n+1} = X_n .$$

Then the target size was fixed at ε_t, and the above targeting algorithm was applied for each source-target pair using p as the controlling parameter ($p_0 = 1.4$). The calculated time required to get the target was averaged over an ensemble of the source-target pairs at fixed target size ε_t. The results of the numerical experiment are presented in Fig. 5.9. The solid line with slope $\lambda_1^{-1} + |\lambda_2|^{-1}$, predicted by (5.24), agrees with the obtained data. The dashed line corresponds to the power law (5.20) with $D \cong 1.26$ (the fractal dimension of the Hénon attractor). The variation of the parameter in realizing the targeting procedure did not exceed 0.1 % of its initial value.

Peculiarities of the targeting procedure in Hamiltonian systems will be considered in the next section.

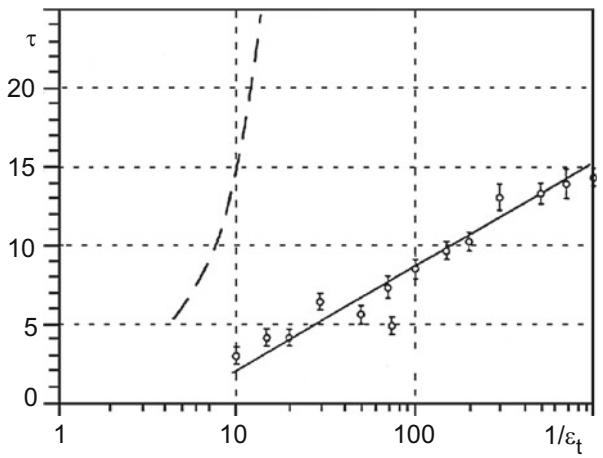

Fig. 5.9 Average time required to get the target of definite size (ξ_t); *solid line* shows the time defined by the relation (5.6), *dotted line* is the time in the absence of targeting [power law (5.1)] [23]

5.6 Chaos Control in Hamiltonian Systems

In this section we will consider an OGY method generalization that allows the realization of chaos control in Hamiltonian systems [26]. There are several reasons that make this generalization a non-trivial task.

Because of the phase volume conservation in Hamiltonian systems, some unstable periodic orbit components have the Jacobi matrix with complex eigenvalues. It makes it impossible to use the formulae (5.11), (5.13), expressed in terms of real eigenvalues immediately for control. We can utilize the unmodified OGY algorithm if we apply the controlling perturbation only over the period, i.e., on each mth step, if the periodic orbit has period m. However, the stabilized chaotic orbit, affected by noise, can deviate from the target orbit before the next perturbation will be applied, and control over the trajectory will be lost. Therefore, for a real system, where noise is always present, an efficient control algorithm must allow control on each time step. The initial control algorithm needs to be slightly modified. Let us do it for the two-dimensional mapping $\mathbf{Z}_{n+1} = \mathbf{F}(\mathbf{Z}_n, p)$ with the usual limitation, imposed on the smallness of the parameter p perturbation. The linearized dynamics in the vicinity of the period-m orbit ($\mathbf{Z}_{01} \to \mathbf{Z}_{02} \to \ldots \mathbf{Z}_{0m} \to \mathbf{Z}_{0(m+1)} = \mathbf{Z}_{01}$) reads:

$$\mathbf{Z}_{n+1} - \mathbf{Z}_{0(n+1)}(p_0) = \hat{A}(\mathbf{Z}_n - \mathbf{Z}_{0n}(p_0)) + \mathbf{B}\delta p_n \,. \tag{5.26}$$

Here we will not, as we did before, express the matrix $\hat{A}$ in terms of its eigenvectors and eigenvalues, as they can be complex in some points of the periodic orbit. Instead, we shall use stable and unstable directions, connected with each periodic orbit component. If $m \neq 1$, then these directions do not necessarily coincide with the eigenvectors of the Jacobi matrix at the same point. The algorithm for determining the stable and unstable directions for periodic orbit components in two-dimensional mappings can be found in [26].

Suppose $\mathbf{e}_{s(n)}$ and $\mathbf{e}_{u(n)}$ are, respectively, stable and unstable directions in the point of the periodic orbit Z_{0n} , and $\mathbf{f}_{s(n)}$, $\mathbf{f}_{u(n)}$ are two vectors satisfying the conditions

$$\begin{aligned} \mathbf{f}^T_{u(n)}\mathbf{e}_{u(n)} &= \mathbf{f}^T_{s(n)}\mathbf{e}_{s(n)} = 1 \\ \mathbf{f}^T_{u(n)}\mathbf{e}_{s(n)} &= \mathbf{f}^T_{s(n)}\mathbf{e}_{u(n)} = 0 \,. \end{aligned} \tag{5.27}$$

For the stabilization of an unstable periodic orbit we require that the point, which, as the result of evolution appeared in small vicinity of some periodic orbit component $\mathbf{Z}_{0n}$, will, on the next $(n+1)$ iteration, get on the stable direction of the component $\mathbf{Z}_{0(n+1)}$. It means that

$$\mathbf{f}^T_{u(n+1)}\left(\mathbf{Z}_{n+1} - \mathbf{Z}_{0(n+1)}(p_0)\right) = 0 \,. \tag{5.28}$$

Projecting the relation (5.26) on the direction $\mathbf{f}^T_{u(n+1)}$ and using the condition (5.28), we get [26]:

$$\delta p_n = -\frac{\mathbf{f}^T_{u(n+1)}\left[\hat{A}\delta\mathbf{Z}_n(p_0)\right]}{\mathbf{f}^T_{u(n+1)}\mathbf{B}}; \quad \delta\mathbf{Z}_n(p_0) = \mathbf{Z}_n - \mathbf{Z}_{0n}(p_0)\,. \tag{5.29}$$

This formula represents an analogue of the relation (5.11) for the OGY chaos control method in Hamiltonian systems. So for the case of the unstable fixed point stabilization $\mathbf{f}^T_{u(n+1)} = \mathbf{f}^T_u$, $\mathbf{f}^T_u\hat{A} = \lambda_u f^T_u$ the relation (5.29) also transforms into (5.11). It is important to note that the parameter perturbation (5.29) is applied to the system on each time step, which minimizes the influence of external noise.

The obtained algorithm was applied in [27] for chaos control in a version of the already considered standard mapping

$$\begin{aligned} X_{n+1} &= (X_n + Y_n) \bmod 2\pi \;\; - \pi \\ Y_{n+1} &= Y_n + p\sin(X_n + Y_n)\,, \end{aligned} \tag{5.30}$$

using p as the controlling parameter. Figure 5.10 shows the results of control for the period-10 unstable periodic orbit. Anomalously long control setup times—about 10^4 iterations—are striking. This is one more difficulty in the realization of OGY control in Hamiltonian systems. In dissipative chaotic systems the average control setup time $\langle\tau\rangle$ is always finite. It is connected with the exponential decay of the distribution function $P(\tau)$ on long times [28]

$$P(\tau) \sim \exp\left[-\tau/\langle\tau\rangle\right]\,. \tag{5.31}$$

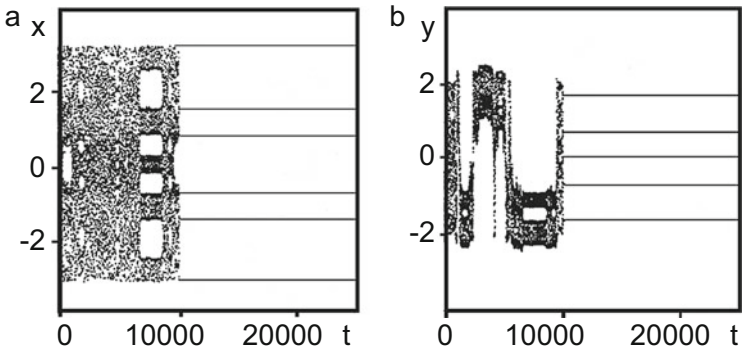

Fig. 5.10 OGY control for the period-10 unstable periodic orbit in the standard mapping (5.30). Only some of the lines corresponding to the periodic orbit are shown. Other lines, when projected on the corresponding planes, have coordinates that coincide with the plotted ones [26]

In Hamiltonian systems, the corresponding distribution function decays considerably slower on long times [29]

$$P(\tau) \sim \tau^{-\alpha}; \quad 1 < \alpha < 2\,. \tag{5.32}$$

This leads to the fact that the average control setup time in Hamiltonian systems

$$\langle \tau \rangle \sim \int \tau^{1-\alpha} d\tau\,, \tag{5.33}$$

tends to infinity. The physical reason for such distribution function behavior is the sticking effect of the trajectory to the invariant tori surviving in the phase space. Therefore, efficient control in Hamiltonian systems can be realized only under conditions of considerable abridgement of the control setup time.

Let us briefly cite one of ways to solve that problem, proposed in the paper [27]. For explanation of the method the authors used the following analogy. Suppose in some mountainous country you must get from one valley to another. If you are not acquainted with the landscape and try to achieve the goal by the random walking, then the march will take a considerable time. The required time can be remarkably shortened if you use the passes connecting the neighboring valleys. Therefore, the authors named their method the pass targeting method.

Let us explain it using the example of two-dimensional Hamiltonian mapping. The phase space structure of a system corresponding to such a mapping in the region of transition from absolute regularity to complete chaos represents a chain of resonance overlaps [30]. This picture is schematically illustrated in Fig. 5.11, where two overlapping resonances are shown. Each resonance is associated with an orbit of a certain period. For example, the unstable fixed point (the saddle point P) is associated with the period-1 resonance (lower hatched region in Fig. 5.11), and the unstable period-2 orbit (the saddle points P_1 and P_2)—with the period-2 resonance (upper hatched region in Fig. 5.11). To transition from one resonance to another, it is necessary to intersect the region of neighboring resonance overlap. This is the pass

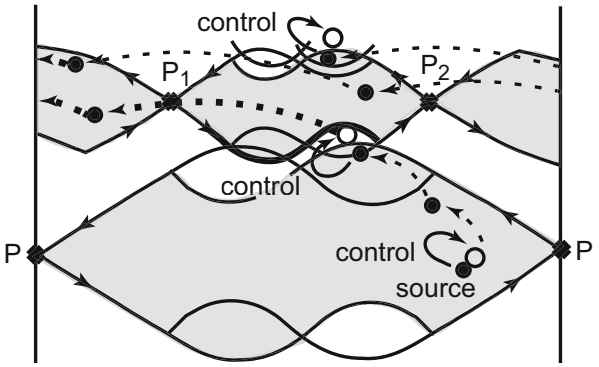

Fig. 5.11 Targeting procedure in a Hamiltonian system [standard mapping (5.30)] in the case of two overlapping resonances [27]

used in the above analogy. Thus, the targeting procedure in Hamiltonian systems must have a multistage character. As the intermediate target on each stage one can choose the neighboring resonance overlap region. The authors of the method checked its efficiency on the standard mapping (5.30). The average time to reach the target, separated from the source by seven resonances for 50 sets of initial conditions, chosen in the chaotic region using the targeting procedure, was within the limit of 125−132 iterations. The uncontrolled transport time for the same source-target combination was from 1119 to 3.77 million iterations.

As a realistic example of the targeting procedure realization in Hamiltonian systems we shall briefly mention the so-called restricted three-body problem [31]: the description of the motion of a light body in the gravitational field of two other bodies, significantly exceeding it in mass. The heavier bodies turn around the common center of gravity under action of mutual attractive forces. Such a model can be used to describe spaceship dynamics in the Earth–Moon gravitational field. The solution obtained in framework of such a model is used for the zero approximation. Subsequent approximations account for the influence of the Sun and other planets.

Let our goal be to transfer the spaceship from a near-earth orbit to a circumlunar one. The straightforward way to achieve that goal is to accelerate the spaceship in order to let it leave the near-earth orbit and then to slow it down for the capture by the Moon's gravity field.

A very different approach [32] is based on the existence of a chaotic sea between the Earth and the Moon (due to the stochasticity of the reduced three-body problem). In that case, a small quantity of rocket fuel can be used to transfer the spaceship from the near-earth orbit into the chaotic sea. Then the spaceship can reach the vicinity of the circumlunar orbit without any fuel losses. However it will take very long time—about 27 years. Using the above targeting procedure in a Hamiltonian system, this time can be shortened to 293 days with multiplied fuel savings [27].

5.7 Stabilization of the Chaotic Scattering

In the present section we will, following [33], consider one more example of controlled Hamiltonian dynamics, but now for cases of infinite motion—chaotic scattering. This represents a type of scattering at which arbitrarily small changes of input variables can result in considerable output changes. In other words, as in any chaotic process, chaotic scattering is characterized by an anomalous sensitivity to initial conditions.

We begin by formulating the problem. An arbitrary particle impacting the scatterer will, generally speaking, stay only a finite time in the scattering region. However, in many important applications (chemical and nuclear reactions, channeling relativistic particles in crystals) it is necessary to keep the particle in the scattering region for longer. Therefore, we naturally come to the following: how can we keep a particle inside the scattering region as long as needed, using only small variations in the system parameters? This task is equivalent to the problem of unstable periodic orbit stabilization inside the scattering region.

Below we will briefly discuss this problem in application to the non-hyperbolic chaotic scattering in Hamiltonian systems. The term "hyperbolic scattering" means scattering in a case when all the periodic orbits are unstable and the invariant tori are absent in the scattering region. At the same time the term "non-hyperbolic chaotic scattering" describes the situation when the surviving invariant tori coexist with the chaotic invariant sets.

Control of non-hyperbolic chaotic scattering has two characteristic features. First let us remember that for strange attractors, the probability of finding a particle in a small vicinity of the target periodic orbit equals unity. However, in the case of chaotic scattering the invariant chaotic set is not an attractor. Therefore, in order to get a finite probability of finding a particle in the vicinity of the target orbit, we should prepare the ensemble of initial conditions, corresponding to motion towards the chaotic set.

Another peculiarity is immediately connected to the non-hyperbolic character of the scattering. If the target unstable periodic orbit is situated far from the invariant tori present in the scattering region, the latter will only slightly affect the average control setup time. However, if the orbits situated near the surviving tori are stabilized, the sticking effect mentioned in the previous section may appear significantly stronger than in the first case.

Let us study the possibility of controlling the chaotic scattering in a simple model, describing the one-dimensional dynamics of a particle driven by δ-like pulses [34]. As the controlling parameters in this model we can use the intensity of the pulses and the time interval between two consecutive collisions. The Hamiltonian of the model reads

$$H(x,p,t) = \frac{p^2}{2m} + T_0 G(x) \sum_{i=-\infty}^{\infty} \delta(t - T_i)\,, \tag{5.34}$$

where T_0 is a constant, The sequence $\{T_i\}$ determines the moments of the pulses, and $T_0 G(x)$ is the pulse amplitude at point x. Suppose $\{x_n, p_n\}$ are the dynamical variables of the particle before the nth pulse. Then, immediately before the $(n+1)$th pulse, those dynamical variables are defined by the following Hamiltonian (area-preserving) mapping:

$$\begin{aligned} p_{n+1} &= p_n - T_0 \frac{dG(x_n)}{dx_n} \\ x_{n+1} &= x_n + T_n P_{n+1}\,, \end{aligned} \tag{5.35}$$

where T_n is the time interval between nth and $n+1$th pulse.

In order to make the model (5.34) describe the scattering dynamics, we should take the function $G(x)$ such that the derivative $dG(x)/dx$ turns to zero over long distances. Let us choose $G(x)$ in the form

$$G(x) = D(1 - e^{-\alpha x})^2\,, \tag{5.36}$$

where D, α are free parameters. After the following scaling transformation:

$$p_n \to p_n/(\alpha T_0), \quad x_n \to x_n/a$$

the mapping (5.35) takes the form

$$\begin{aligned} p_{n+1} &= p_n - d\left(e^{-x_n} - e^{-2x_n}\right) \\ x_{n+1} &= x_n + \frac{T_n}{T_0} p_{n+1}\,, \end{aligned} \tag{5.37}$$

where $d = 2\alpha^2 T_0^2 D$.

As was shown in [33], the mapping (5.37) demonstrates different types of dynamical behavior depending on the values of the parameters d and T_n. In particular, for $T_n = T_0$ the mapping reproduces both hyperbolic and non-hyperbolic scattering at different values of d. In the case $0 < d < d_c \approx 4.58$ the scattering is non-hyperbolic, because the phase space contains the invariant tori. Figure 5.12

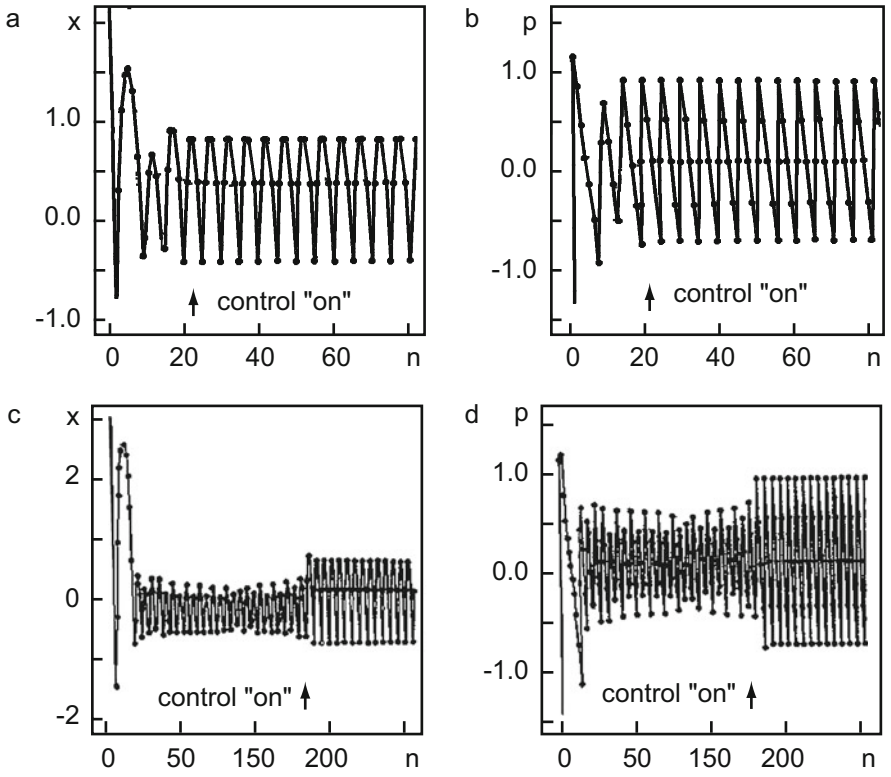

Fig. 5.12 Two examples of the OGY control for the chaotic scattering [33] in the model (5.37). (**a**), (**b**): $X_0 = 8,\ P_0 = -4.398$; (**c**), (**d**): $X_0 = 8,\ P_0 = -9.072$

presents the results of control for period-5 unstable periodic orbit ($d = 1.8$) with the algorithm (5.29) for two sets of initial conditions. The relatively longer period of control setup in the second case is connected with influence of the surviving invariant tori, mentioned above.

5.8 Control of High-Periodic Orbits in Reversible Mapping

In the present section we will demonstrate the efficiency of the discrete parametric control method for the stabilization of high-period orbits in reversible mappings, which we introduced in Chap. 4. As was mentioned above, the specific feature of these systems is that the basic elements of Hamiltonian systems (e.g., resonances) and those of the dissipative systems (e.g., attractors) can coexist in their phase space [35, 36]. The coexistence of those elements broadens the circle of physical phenomena which can be realized in reversible systems compared with Hamiltonian or dissipative ones.

Let us consider a simple reversible system—two-dimensional two-parametric (a, ε) mapping, describing the discrete dynamics of a linear oscillator subject to δ-like pulses with the stiffness coefficient proportional to the velocity:

$$\mathbf{r}_{n+1} = \begin{pmatrix} x_{n+1} \\ y_{n+1} \end{pmatrix} = \mathbf{F}(\mathbf{r}_n) = \begin{pmatrix} x_n + y_{n+1} \bmod 2 \\ y_n - \varepsilon(a - y_n)x_n \end{pmatrix} . \tag{5.38}$$

The phase space for this mapping is the cylinder $x \in (-1, 1)$, $y \in R$; the values $x = -1$ and $x = 1$ are identified. The variable x_n plays the role of the angular coordinate. The mapping (5.38) has fixed points $P_k^s = \left(x_k^s, y_k^s\right)$, where $x_k^s = 0$ and $y_k^s = 2k$ ($k = \pm 1, \pm 2, \ldots$; $a \neq 2k$). For fixed values of ε and a the solutions of the characteristic equation

$$\lambda^2 + \lambda \mathrm{SpA} + \det A = 0 , \tag{5.39}$$

determine the type of the fixed points. Here $A(\mathbf{r}_k) = (\partial \mathbf{F}/\partial \mathbf{r})_{\mathbf{r}=\mathbf{r}_k}$ is the Jacobi matrix of the mapping (5.38). The characteristic equation (5.39) is obtained as the result of linearization of (5.38) in vicinity of the fixed point. It easy to see that

$$\det A = 1, \qquad \mathrm{SpA} = 2 - \varepsilon \left(a - y_k^s\right) . \tag{5.40}$$

A compact classification of fixed points depending on the SpA and $\det A$ values is presented in Fig. 5.13. The condition $\det A = 1$ means that there are only hyperbolic (saddles) or elliptic (centers) fixed points, that is, precisely those phase space elements which exist in Hamiltonian systems. The phase portrait of the mapping (5.38) contains one more important element absent in Hamiltonian

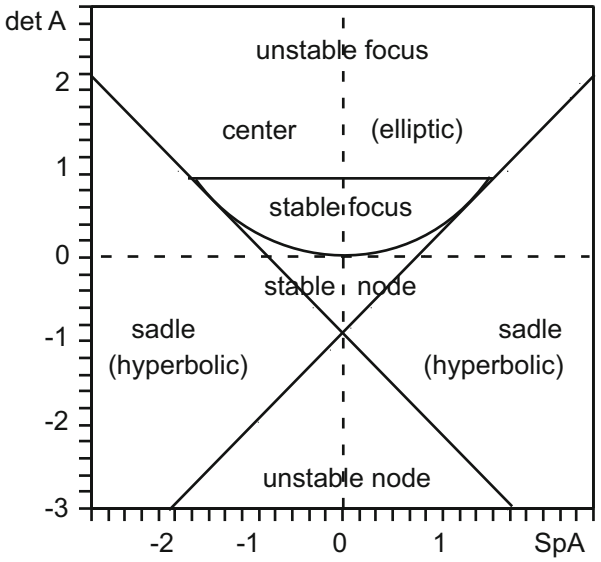

Fig. 5.13 Compact classification of fixed points depending on the SpA and det A values

systems—the invariant set consisting of the family of singular solutions

$$y_n = a, \quad x_{n+1} = (x_n + a) \mod 2\,. \tag{5.41}$$

For the fixed value of a each one of the solutions (5.41) (they differ one from another in the choice of the initial condition x_0) represents a periodic or quasi-periodic trajectory for rational and irrational values of a, respectively. For $\varepsilon < 1$ the invariant set (5.41) attracts nearby trajectories with the increment $\gamma \cong \frac{\varepsilon^2}{6}$ and therefore it can be considered an attractor [36]. The region of attraction to the attractor has a complicated fractal structure. Along with the regular component, the phase space of the mapping (5.38) also contains a chaotic one. The scenario of the transition to chaos in reversible systems is distinct from those that are observed both in dissipative and Hamiltonian systems. On the one hand, it is connected to the absence of a strange attractor, and on the other hand, to the fact that the trajectories are attracted by the attractor at $y_n = a$ for any arbitrarily small ε value, that does not allow to realize in full measure the resonance overlapping scenario [37], characteristic for Hamiltonian systems. Interaction of the attractor with the periodic trajectories, surrounding the elliptic fixed point, determines the specifics of transition to chaos in the considered mapping. Figure 5.14a shows a fragment of the considered mapping with a stability island in vicinity of the point $(x, y) = (0, 0)$. As the island and the attractor come together, i.e., at the decreasing of the parameter a (Fig. 5.14b), the destruction of high-order resonance separatrices and the formation of the stochastic layer takes place (Fig. 5.14c). Numerical calculations [38] show

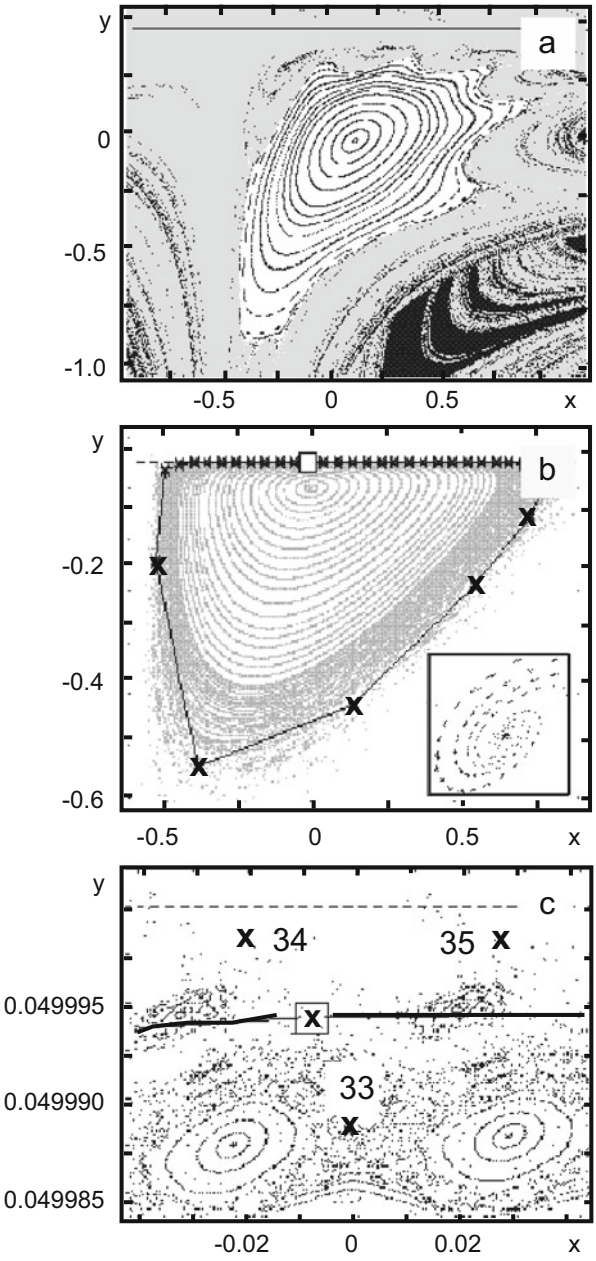

Fig. 5.14 (**a**) A fragment of phase space of the mapping (5.38) with a stability island in vicinity of the point $(x, y) = (0, 0)$; (**b**) deformation of the stability island at its approach to the attractor; (**c**) destruction of high-order resonances separatrices and formation of the stochastic layer for the unstable periodic orbits with $k = 34$ [a fragment of the phase space corresponding to the *white square* on (**b**)]

that at $k \sim 30$ (k is the order of resonance or of the orbit) for $a = 0.05$ widths of the resonances and distances between them become of the same order. According to Chirikov's criterion of non-linear resonances, this means that in the region of higher k values the transition to global stochasticity must be observed. However, unlike Hamiltonian systems, where the resonance width is determined only by the non-integrable perturbation amplitude, in reversible mapping (5.38) the reason of the transition to chaos is the approach (interaction) of Hamiltonian and dissipative phase space elements: namely of the stability island and of the attractor.

Even this simple analysis allows the dynamical system (5.38) to be related to the class of the so-called complex systems [39], which are characterized by the following main features:

1. a complex system is structurally inhomogeneous;
2. individual components of a complex system can be both regular and chaotic;
3. a complex system has a space-time scale hierarchy.

Because of this structural complexity, we can expect that even a weak perturbation applied to the system results in transitions between the different components. Therefore, it seems natural to use the parametric control method to stabilize chaotic regimes in reversible mappings like (5.38) [38, 40].

Before discussing the control problem, we need to find an adequate method for localizing the unstable high-period orbits that interest us. The traditional methods based on the Newton–Rafson procedure are not efficient in cases of unstable orbits because they require highly precise initial conditions needed to perform the iteration procedure. An alternative method [11], which was already mentioned above, implies the preliminary linear transformation of coordinates, which transforms the unstable periodic orbits into stable ones, preserving their position in space. After that, the position of the stable periodic orbits (in new coordinates) can be determined with the help of simple iteration procedures. For the considered two-dimensional mapping, the coordinate transformation has the following form:

$$\mathbf{r}_{n+1} = \mathbf{r}_n + \Lambda_i \left[\mathbf{F}^k(\mathbf{r}_n) - \mathbf{r}_n \right] ,$$

where k is the period of the considered orbit ($\mathbf{r} \to \mathbf{r}_2 \to \ldots \mathbf{r}_k \to \mathbf{r}_{k+1} = \mathbf{r}_1$), Λ_i is one of $\alpha_2 = 8$ ($i = 1, 2, \ldots, 8$) reversible 2×2 matrices. In D-dimensional space $\alpha_D = D!2^D$. The concrete form of Λ_i is determined by type of the corresponding unstable point. The inset in Fig. 5.14b demonstrates an example of the transformation that transfers the saddle point into a stable focus. As a control object we take the unstable periodic orbit of the mapping (5.38) with $k = 34$, lying at $a = 0.05$ in the global stochasticity region (see Fig. 5.14c). For stabilization we will use the main formula of the discrete parametric control (5.11), taking as p one of the parameters a or ε. Figure 5.15 shows in action the basic mechanism of the used control method. We took four trial points (black squares) in the vicinity of a randomly chosen saddle point, belonging to the period-34 unstable orbit. The trajectories of the four trial points are shown after three consecutive iterations. After the third iteration all four trial points are already lined up along the stable

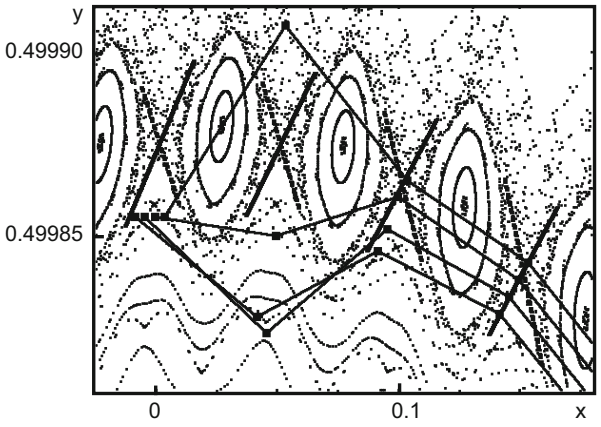

Fig. 5.15 OGY control mechanism: temporal evolution of four trial points

direction. After consecutive iterations they stay on the stable direction approaching the saddle point after each iteration. Figure 5.16 shows the behavior of the deviation $\left|\mathbf{r}_n - \mathbf{r}_n^*\right|$ of the system position $\mathbf{r}_n$ from the periodic orbit $\mathbf{r}_n^*$. We use a logarithmic scale in order to follow all the control stages: the chaotic oscillations preceding the control setup, the exponentially fast approach to the target period orbit, the stable motion along the periodic orbit $\left|\mathbf{r}_n - \mathbf{r}_n^*\right| \sim 10^{-15}$, the exponentially fast deviation from the target orbit after turning off the control, and the restitution of the chaotic oscillations. As in the previously considered cases of the OGY control of dissipative and Hamiltonian systems, the analogous reversible system control method appears to be relatively steady with respect to external noise. Figure 5.16b gives the result of the control with the inclusion of the term $s\boldsymbol{\xi}_n$ on the right-hand side of the mapping (5.38). The components $\xi_{x,y;n}$ represent independent Gaussian random variables with zero mean and unit dispersion. The action of noise considerably lowers the control efficiency, but even in this case the method allows us to keep the chaotic trajectory in the vicinity of the unstable periodic orbit during the time period of almost the same order of magnitude as in the absence of noise. At first glance it seems that the results of the high-period orbits control in the reversible mapping are quite similar to the corresponding results for the Hamiltonian systems. However, more careful consideration [40] shows that the coexistence of attractor and stability islands, which is a characteristic feature of reversible systems, substantially complicates the situation. As it was mentioned many times previously, the control is turned on only when the trajectory $\mathbf{r}_n$ gets into a region sufficiently close to the target periodic orbit. Let us call it the capture region. The capture region size and its shape are determined by the maximum admissible value of the controlling parameter deviation $\delta p_{\max}$ from its nominal value and by local characteristics of the periodic orbit. The basic formula of OGY control (5.11) can be presented in the form

$$\delta p_n = M_i \delta x_n + N_i \delta y_n; \quad i = (n) \bmod k\,.$$

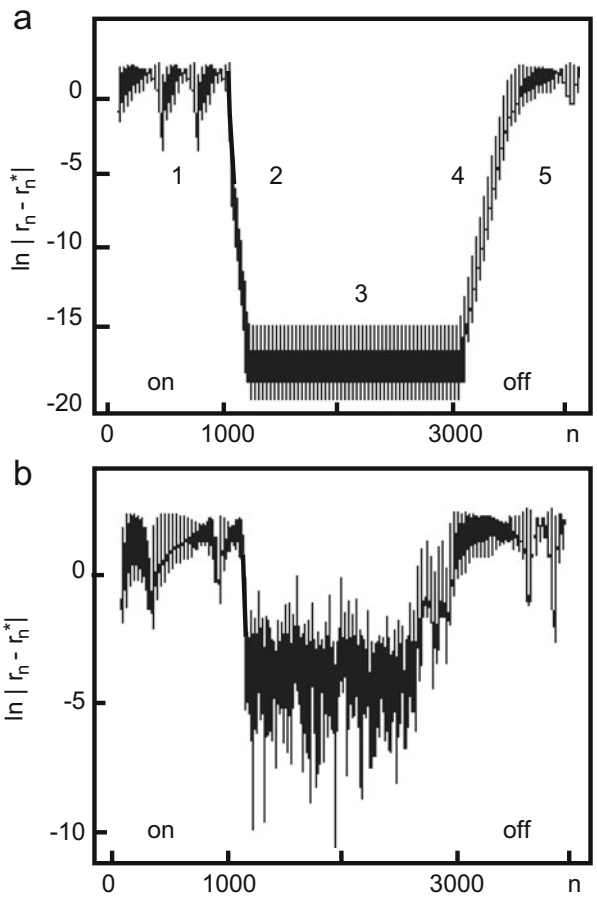

Fig. 5.16 Result of the OGY control of the mapping (5.38): (**a**) without noise; (**b**) with Gaussian noise

The coefficients M_i and N_i can be obtained from (5.11) in explicit form. The capture region for any ith point of the periodic orbit is determined by the condition

$$|M_i \delta x + N_i \delta y| < \delta p_{\max} .$$

It is evident that the capture region size determines both the control setup time and the critical amplitude of noise destructing the control. As numerical calculations show, areas of the capture regions of the considered period-34 unstable orbit differ in several orders of magnitude. Such situation is typical for generic periodic orbits in complex (in the sense of the above definition of complexity) dynamical systems. Accounting for this, for orbits with considerably different capture regions it may be convenient to introduce the concept of local and global control [40]. In the case of

local control, the condition $|\delta p_n| < \delta p_{\max}$ is satisfied only for some points of the periodic orbit, whereas in the case of global control, it is satisfied for all points. It is evident that there is no difference between local and global controls for the fixed points and for the periodic orbits with capture regions approximately equal for all points of the orbit. On the contrary, for unstable periodic orbits with substantially different capture regions, global control takes place only in cases when the local control condition is satisfied for the points with the minimal capture area. From the point of view of control realization, those points can be called the dangerous ones. For the considered period-34 orbit the dangerous points constitute less than 30 % of the total number of points forming the periodic orbit. The strategy relying on the local control setup for the dangerous points will automatically lead to a global control setup as well, and it will allow to substantially lower computational efforts.

5.9 Controlling Chaos in Time Dependant Irregular Environment

The above considered schemes of the chaos control are immediately applicable to the systems where the noise is relatively small, i.e., it does not interfere with the structure of the initial phase space. Let us now turn to a principally different situation, when the system is in contact with a time dependent environment (a medium). As the environment we shall understand some large dynamical system, whose evolution does not depend on the controlled system, but strongly affects the latter.

Our goal is to adapt the OGY control technique for cases where the medium changes irregularly and short-term predictions of the evolution of the medium are possible. The effectiveness of the modified technique [41] will be demonstrated on the following problem: to control and prevent ship upset due to a beam sea (waves running at right angles to the boat's course). Here the ocean waves can be understood as the medium. The control algorithm should admit considerable irregular variations in wave amplitudes and phases.

For a description of the ship driven by a beam sea we shall use the non-linear oscillator model

$$\ddot{x} + \nu\dot{x} + \omega^2(x - \alpha x^3) = W(t)\,, \tag{5.42}$$

where x is the angle of deviation of the ship mast from the vertical, ν is the friction coefficient, ω is the frequency of small oscillations near the potential minimum, α is the non-linearity parameter, and $W(t)$ is the term describing the action of the ocean waves on the ship. In the absence of waves ($W(t) = 0$) at small shifts x the oscillations dampen and the ship returns to the vertical position. For large shifts, the gravitational force exceeds the hydrostatic extrusion and x has a tendency to the attractor situated at $|x| = \infty$. When this happens, we can say that the ship upsets.

Suppose that the irregular wave term $W(t)$ has the form

$$W(t) = f(t)\,[1 + \varepsilon_a g(t)] \sin\phi(t) \equiv F(t) \sin\phi(t)\,, \tag{5.43}$$

where $F(t)$ is the wave amplitude, $f(t)$ is its slowly varying component, $g(t)$ is the fast irregular component, and $\varphi(t)$ is the phase whose evolution is determined by the relation

$$\phi(t) = \Omega + \varepsilon_p h(t)\,, \tag{5.44}$$

where $h(t)$ is also an irregular function of time. As the irregular functions $g(t)$, $h(t)$ we will use the solutions for well-known chaotic systems: the Duffing oscillator [42] and the Rössler system [43]. Under the normalization condition for the functions $g(t)$, $h(t)$ the quantities $\varepsilon_a,\ \varepsilon_p$ serve as the relative measures of amplitude and phase irregularity. The use of low-dimensional chaotic systems to generate the random functions $g(t)$, $h(t)$ is dictated only by considerations of convenience and it does not lead to essential differences from the uses of other random functions or chaotic systems of higher dimensions. For numerical calculations in the model (5.37) we will use the following parameters: $\nu = 0.5, \alpha = 1, \omega = \Omega = 1$.

In the case of purely sinusoidal waves ($\varepsilon_a = \varepsilon_p = 0, f(t) = f_0$) for $0 < f_0 < 0.7$ the ship dynamics is strictly regular: it has periodic oscillations with the period $T = 2\pi/\Omega$. At a further increase of the wave amplitude, the period doubling bifurcations cascade takes place, resulting in the chaotic dynamics of the ship. At $f_0 \approx 0.726$ the boundary of the chaotic attractor is destroyed and almost all the initial conditions get on the attractor $|x| = \infty$, i.e., in the absence of control the ship capsizes at $f > f_0$. As was shown in the paper [41] the use of a slightly modified OGY control procedure allows us to avoid the upset both for purely sinusoidal waves with the amplitude considerably exceeding critical levels and in the case of relatively strong amplitude and phase irregularity $\left(\varepsilon_a \neq 0, \varepsilon_p \neq 0\right)$

The equation of motion for the variable x after turning on the controlling perturbation $C(t)$ has the form

$$\ddot{x} + \nu\dot{x} + \omega^2(x - \alpha x^3) = W(t) + C(t)\,. \tag{5.45}$$

To realize the discrete control in a standard way we transition from the ordinary differential equation (5.45) to a mapping in the Poincaré section plane, defining the latter by the conditions $W(t_n) = 0,\ dW/dt > 0$. We will assume that $C(t)$ does not change between two consecutive intersections of the Poincaré section. In the considered problem the perturbation $C(t)$ can be realized, for example, due to a shift of the ballast with respect to the ship's axis in the moment $t = t_n$. As always, we assume the smallness of the perturbation to be $C(t) \ll W(t)$. To that end, we limit the perturbation by the condition $-C_0 \leqslant C \leqslant C_0$.

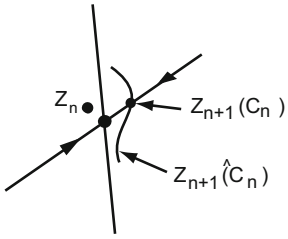

Fig. 5.17 Schematic representation of control in random environment [41]

Let Z_n $(Z = (x, \dot{x}))$ be an unstable fixed point of the Poincaré mapping (see Fig. 5.17) in the moment $t = t_n$ at $\varepsilon_a = \varepsilon_p = 0$, $f(t) = f(t_n)$. Setting $\varepsilon_a \neq 0$, $\varepsilon_p \neq 0$, we introduce irregularity into the wave. Suppose now, that as a result of observations, we can make sufficiently accurate predictions about the behavior of $W(t)$ on the interval $t_n \leqslant t \leqslant t_{n+1}$. Integrating the equation of motion (5.45) with the predicted value $W(t)$ and different values of $\hat{C}$ from the interval $[-C_0, C_0]$, we obtain the system's position in the phase space at the moment $t = t_{n+1}$. To make a decision (on the ballast shift) we will use that value $\hat{C} = C_n$, at which the point Z at the moment t_{n+1} gets on the stable direction of the unstable fixed point.

Figure 5.18 presents the control results in the presence of both amplitude ($\varepsilon_a = 0.15$) and phase ($\varepsilon_p = 0.1$) irregularities for systems where $f(t)$ is the function of time linearly growing from the value $f(0) = 0.7$ to the value $f(300) = 1$. The use of the considered control scheme allows the ship's stability to improve considerably.

5.10 Continuous Control with Feedback

Having devoted sufficient attention to the numerous merits of the OGY method, we will now point out its limitations. The OGY chaos control method is immediately applicable to dynamics described by mappings. By controlling the chaos observable in experimentation, the method reduces the real dynamics to the mapping generated by the Poincaré section, which also determines the discrete character of the controlling parameter variation. Suppose τ is the time interval between consecutive changes to the parameter and λ is the maximal Lyapunov exponent for the target unstable periodic orbit. Then evidently the OGY method is efficient only for those orbits that satisfy the condition

$$\lambda \ll 1/\tau\,. \tag{5.46}$$

The discrete character of the controlling parameter variation also worsens the stability of the OGY method with respect to noise. For relatively rare parameter changes there is a high probability of control failure. Those native disadvantages of discrete control make continuous control realization more attractive. As before, we require the smallness of the controlling perturbation variation because we intend to

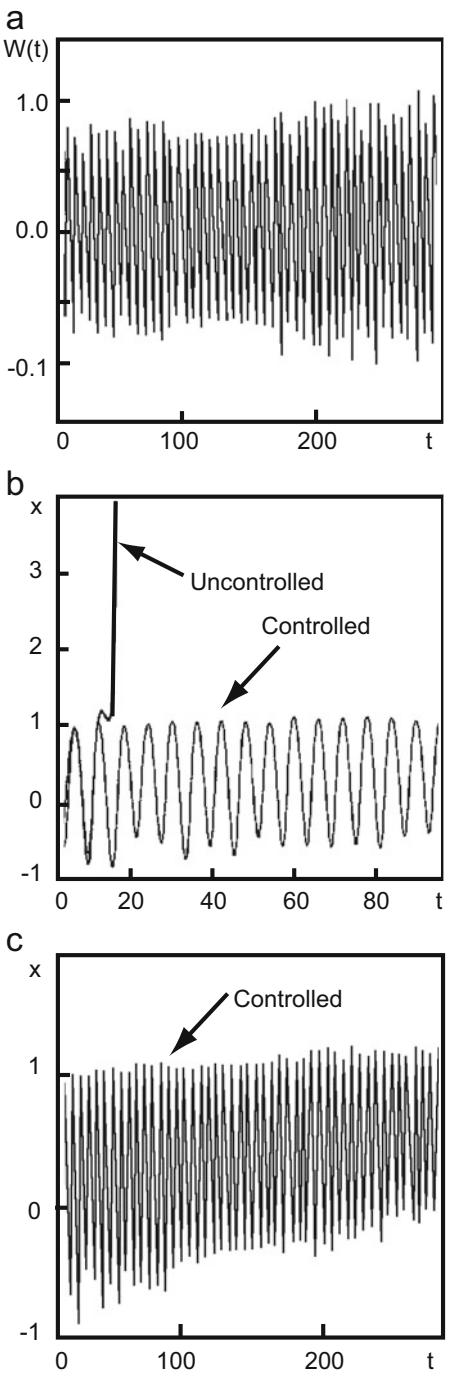

Fig. 5.18 An example of control realization in random environment: (**a**) the perturbation $W(t)$ with parameters $\varepsilon_a = 0.15,\ \varepsilon_p = 0.1$; (**b**) controlled and uncontrolled orbits; (**c**) more extensive segment of the controlled orbit [41]

stabilize the chaotic trajectory in the vicinity of a periodic orbit of the unperturbed system. This goal can be achieved only with a feedback control scheme. The two first continuous control feedback schemes were proposed and realized in the work [44]. Both schemes were based on special constructions of time-continuous perturbation which, without changing the target unstable periodic orbits, under certain conditions stabilize them. The combination of the feedback and the periodic external force lies at the core of the first scheme. The second one does not require any external force, but uses the self-controlled feedback.

We begin with the first scheme: continuous control with external force. Suppose we have a dissipative dynamical system described by some set of ordinary differential equations. Suppose also that the input of the system is available for external force application and we can measure some scalar characteristic on the output. Those assumptions are satisfied by the following model:

$$\begin{aligned} d\mathbf{x}/dt &= Q(\mathbf{x}, y) \\ dy/dt &= P(\mathbf{x}, y) + F(t)\,. \end{aligned} \tag{5.47}$$

Here y is the variable registered on the output, and $\mathbf{x}$ are all other dynamical variables of the system, that are either unavailable for measurement or do not make interest for the observer. We assume for simplicity that the input signal $F(t)$ perturbs only that equation which corresponds to the variable registered on the output. We will also consider that the dynamical system (5.47) in absence of the external force ($F(t) = 0$) has a strange attractor. When working with a real system, exact knowledge of the model (5.47) is not necessary. Using the time delay method described in Chap. 4 we can reconstruct full system dynamics from the observable scalar characteristics. Using this method we can reconstruct various periodic orbits $y = y_i(t)$, $y_i(t + T_i) = y_i(t)$, where T_i is the period of ith unstable periodic orbit. Let us choose from these obtained orbits one which we want to stabilize. Later, we will need an additional oscillator generating a signal proportional to $y_i(t)$. The difference $D(t)$ between $y_i(t)$ and the output signal $y(t)$ will be used as the controlling perturbation

$$F(t) = K\,[y_i(t) - y(t)] = KD(t)\,. \tag{5.48}$$

Here K is the experimentally tunable weight of the perturbation. The perturbation i applied on the system input as the negative feedback ($K > 0$). The flow-chart of the continuous control with external force is represented in Fig. 5.19. For many physical

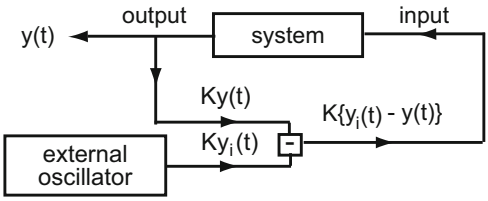

Fig. 5.19 Block-diagram of the continuous control with external force

systems, its experimental realization does not present any difficulty. An important feature of the perturbation choice in the form (5.48) consists of the fact that the perturbed system preserves the initial periodic orbits: $y(t) = y_i(t)$ is a solution of (5.47) with $F(t) = 0$.

The stabilization of the unstable periodic orbit by this control method is achieved by varying the weight factor K. When stabilization is achieved, the output signal $y(t)$ is very close to $y_i(t)$ and therefore, as in the OGY method, only small perturbation is used on the control time interval.

The experimental realization of the considered continuous control version can be divided into two stages. At the first, preliminary, stage we shall study the signal at the unperturbed system output and construct the oscillator generating the signal proportional to $y_i(t)$. At the second stage, the control is carried out by the scheme presented in Fig. 5.19.

Let us demonstrate the efficiency of the continuous control with external force using an example of the Rössler system [43]

$$\begin{aligned} \frac{dx}{dt} &= y - z \\ \frac{dy}{dt} &= x + 0.2y + F(t) \\ \frac{dz}{dt} &= 0.2 + z(x - 5.7)\,. \end{aligned} \tag{5.49}$$

We have chosen $y(t)$ as the scalar signal measured on the system output. The result of control does not depend on the choice of perturbed variable. Figure 5.20 presents the results of the stabilization of the period-5 unstable orbit. The beginning of the curve F corresponds to the moment perturbation is turned on. As expected, after a small transition period, the perturbation becomes small and the system comes to the periodic regime corresponding to the target orbit. The same figure presents the results of the stabilization of the period-2 unstable orbit for the Lorenz system [45]

$$\begin{aligned} \frac{dx}{dt} &= 10(x - y) \\ \frac{dy}{dt} &= -xz + 28x - y + F(t) \\ \frac{dz}{dt} &= xy - \frac{8}{3}z\,. \end{aligned} \tag{5.50}$$

The perturbation amplitude in the control regime depends on two factors: the precision of the unstable periodic orbit $y_i(t)$ reconstruction and the noise intensity. In an ideal case of the system moving along the orbit at zero noise level, stabilization can be achieved with a negligibly small level of the external oscillator signal (see Fig. 5.20).

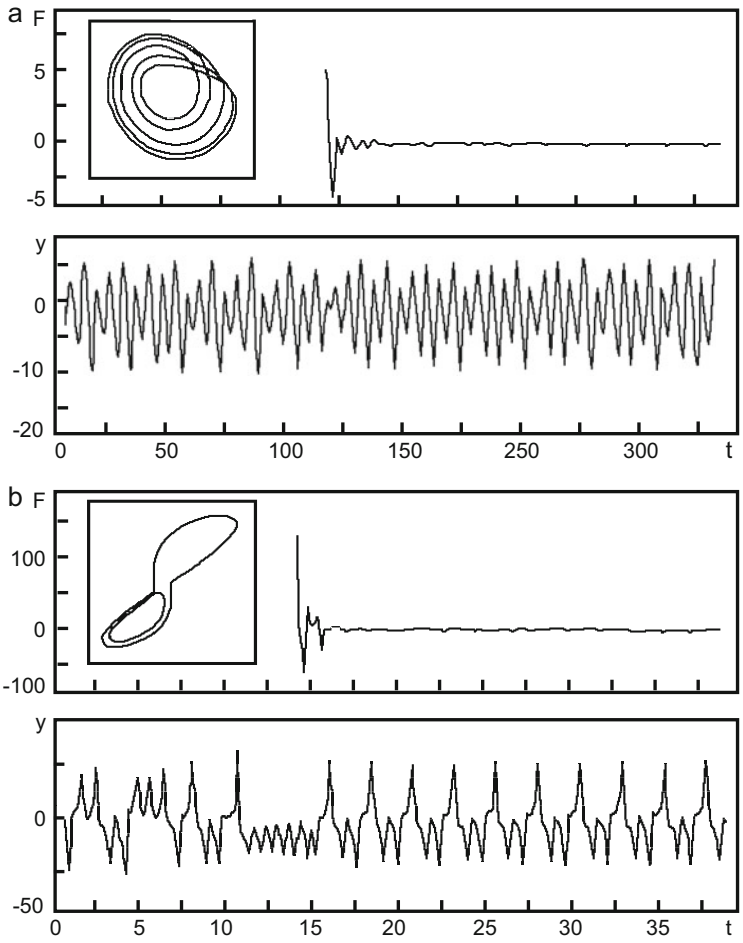

Fig. 5.20 Results of the continuous control with external force: (**a**) output signal $y(t)$ and external force $F(t)$ for the Rössler system (5.49) at $K = 0.4$; (**b**) the same quantities for the Lorenz system (5.50) [44]

Let us now dwell on the influence of noise determining the perturbation amplitude in the control regime. We will again use the Rössler system and introduce on the right-hand sides of equations (5.49) the additional terms $\varepsilon\xi_x(t)$, $\varepsilon\xi_y(t)$, $\varepsilon\xi_z(t)$. Random functions ξ_x, ξ_y, ξ_z are independent from one another and they have zero mean values and unit dispersions. Figure 5.21 presents the results of control for the period-1 orbit in the Rössler system for two different noise levels: $\varepsilon = 0.1, \varepsilon = 0.5$. Because the control is continuous, even for high noise levels on sufficiently long time segments there is no stabilization failure, as can be observed in the discrete control. Increase in noise levels leads only to growth in the controlling perturbation amplitude and to some "smearing" of the periodic orbit.

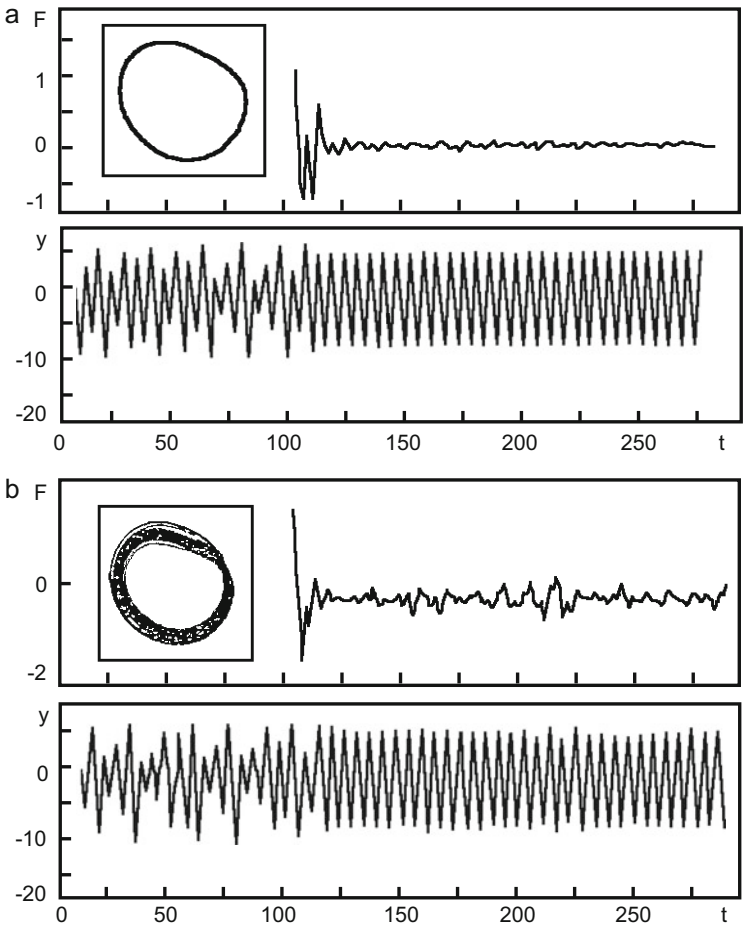

Fig. 5.21 Results of continuous control for the period-1 orbit in the Rössler system (5.49) for two different noise levels at $K = 0.4$: (**a**) $\varepsilon = 0.1$, (**b**) $\varepsilon = 0.5$ [44]

We should note one more important distinction between continuous and discrete control. The former starts to work only if the system is close to the target orbit, as it is based on the linearization of the deviation from it. In the continuous control method there is no need to wait for the approach of the system to the target orbit. The perturbation can be turned on at any time. Thus the Rössler system is efficiently synchronized with the external oscillator even if the initial conditions are far from the periodic orbit. Although, in that case, the initial perturbations increase. However, we should not expect an analogous situation for more complex systems where the stabilized orbits belong to different basins of initial conditions. Such multi-stability substantially complicates the achievement of the goal. A large initial perturbation can also be undesirable for the experiment, the control of which is planned. In

many cases, both problems can be solved by forced limitation of the perturbation. Introducing some non-linear element in the feedback chain allows $F(t)$ to reach saturation for large deviation values $D(t)$:

$$\begin{cases} -F_0, & KD(t) < -F_0, \\ KD(t), & -F_0 < KD(t) < F_0, \\ F_0, & KD(t) > F_0. \end{cases} . \tag{5.51}$$

Here $F_0 > 0$ is the saturating perturbation value. Although the perturbations (5.48) and (5.51) work identically in the vicinity of the stabilized unstable periodic orbit, they lead to distinct transition processes. In the case of (5.51) the perturbation is always small (at small F_0), including the transition process; however, the latter considerably increases in average. The system "waits" until the chaotic trajectory approaches the target orbit sufficiently closely, and only after that synchronizes it with the external oscillator. As in the discrete control method the average duration of the transition process grows quickly with decrease of F_0.

In order to analyze the local stability of the system in the control regime it is useful to calculate the maximal Lyapunov exponent. To do that we use the example of the Rössler system (5.49), linearized in small deviations from the target periodic orbit. The dependence of the maximal Lyapunov exponent λ on the parameter K for period-1 and period-2 orbits is presented in Fig. 5.22. Negative values of the Lyapunov exponent $\lambda(K)$ determine the interval K, corresponding to the stabilized unstable periodic orbits. For the Rössler system the period-1 orbit is stabilized on the finite interval $[K_{\min}, K_{\max}]$. Values of $K_{\min}$ and $K_{\max}$ determine the stabilization threshold: $\lambda(K_{\min}) = \lambda(K_{\max}) = 0$. The period-2 orbit has infinite stabilization interval. The Lyapunov exponent $\lambda(K)$ for both orbits has a minimum at some value $K = K_{\text{op}}$, providing the optimal control. We should note that the control interval size $K_{\max} - K_{\min}$ depends on the choice of controlled variable. So, for example, for the Rössler system, the control of the y variable is the most efficient, because this choice leads to the maximal interval corresponding to stabilization. Some systems can have several stabilization intervals for the same variable. Thus the Lorenz system in the

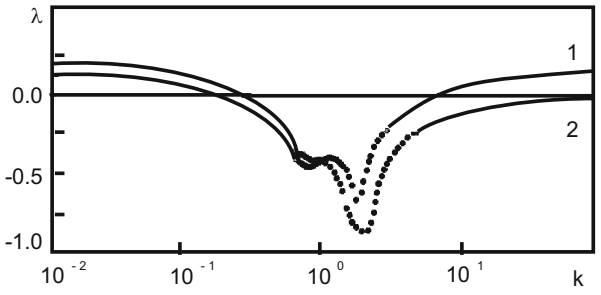

Fig. 5.22 Dependence of the maximal Lyapunov exponent λ on the parameter K for period-1 and period-2 orbits in the Rössler system [44]

case of z variable control has two isolated stabilization intervals. The presence of the threshold $K_{\min}$ is well understood: the perturbation must be sufficiently strong in order to compensate for the divergence of trajectories close to the unstable orbit, i.e., to invert the λ sign. However, large values of K worsen the control. This is connected with the fact that in the considered realization of continuous control the perturbation acts immediately only on one of the system variables. For large K those perturbations change so quickly in time that the other variables do not have time to follow those changes. The analysis shows that in the multi-parametric control version, when perturbation is introduced in each of the equations of motion, the monotonous decrease of $\lambda(K)$ is observed and the second threshold for $K_{\max}$ is absent.

The latter observation leads to the following question (particularly important for experimental realization of the continuous control): in what chaotic systems is single-parametric control efficient? The answer is based on the assumption that stabilization is possible only in cases where perturbation has a number of degrees of freedom sufficient to suppress the exponential divergence in all available directions. In other words, the minimal number of the controlled variables must be equal to the number of the positive Lyapunov exponents in the controlled system. The chaotic systems, where two or more Lyapunov exponents are positive, are called hyper-chaotic. No version of single-parametric control makes possible the stabilization of hyper-chaotic systems. At the same time, however, the multi-parametric control is efficient for such systems.

The complexity of experimental realizations of the above control method is due to the presence of the special external oscillator. An alternative continuous control method—continuous control with delayed feedback—is free of that weak point. The method replaces the external signal $y_i(t)$ in (5.48) with the delayed output signal. In other words, we will use the controlling perturbation in the form

$$F(t) = K\left[y(t-\tau) - y(t)\right] = KD(t)\,, \tag{5.52}$$

where τ is the delay time. If this time coincides with the period of ith periodic orbit $\tau = T_i$, then the solution of the system (5.47) will also correspond to that periodic orbit, i.e., $y(t) = y_i(t)$. It means that the perturbation of the form (5.52), as well as (5.48), does not change the periodic orbits in the system. Choosing the appropriate weight K of the feedback, we can achieve the stabilization of the system. The block-diagram corresponding to this version of the continuous control method is presented in Fig. 5.23.

The results of the period-3 orbit in the Rössler system and period-1 orbit in the non-autonomous Duffing oscillator

$$\frac{dx}{dt} = y,\ \frac{dy}{dt} = x - x^3 - dy + f\cos\omega t + F(t)\,, \tag{5.53}$$

are presented in Fig. 5.24. The situation is very similar to the case considered above of continuous control with external force. However, now the experimental realization is much simpler, as it does not require any external periodic perturbation.

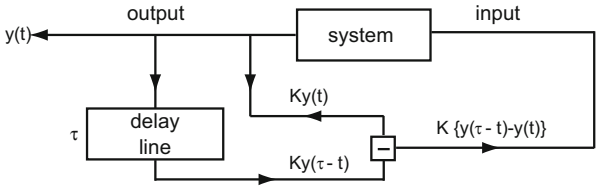

Fig. 5.23 Block-diagram of the continuous control with delayed feedback

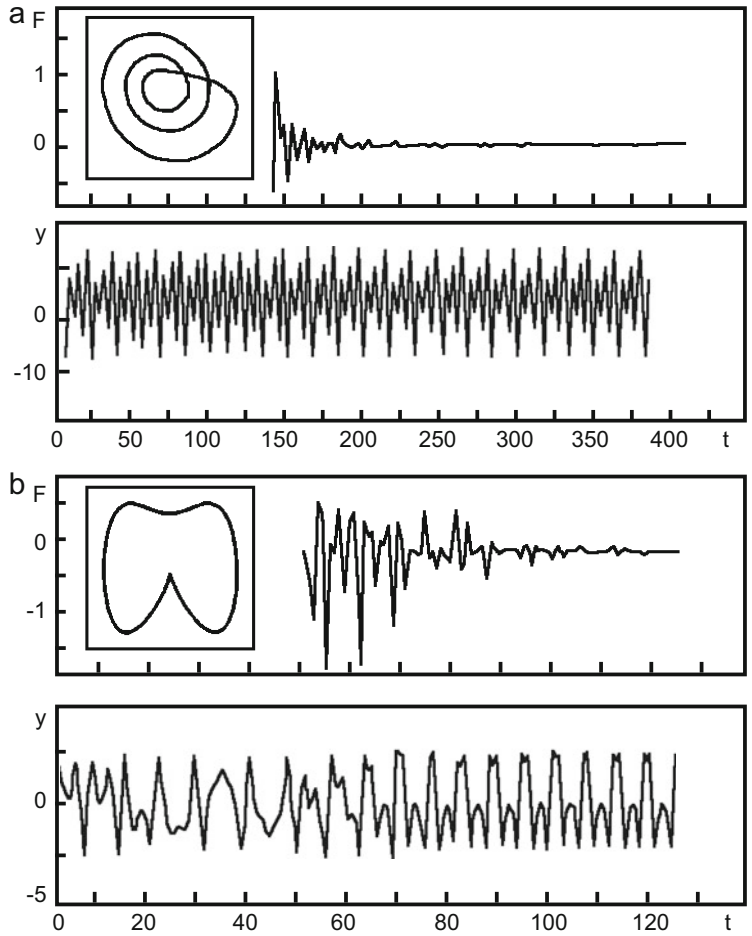

Fig. 5.24 Stabilization of unstable periodic orbits using the continuous control with delayed feedback: (**a**) a period-3 unstable orbit for the Rössler system ($K = 0.2,\ \tau = 17.5$); (**b**) period-1 unstable orbit for the non-autonomous Duffing oscillator ($f = 2.5,\ \omega = 1,\ d = 0.2,\ K = 0.4,\ \tau = 2\pi/\omega$) [44]

The difference between the delayed output signal and the proper output signal is used as the controlling perturbation. This feedback works as the self-control. Only a simple delay chain is needed for its experimental realization. In order to achieve the target unstable periodic orbit stabilization two parameters must be available for tuning in the experiment process: the delay time τ and the feedback weight K. The feedback signal amplitude can be considered as a criterion of the unstable periodic orbit stabilization. When the system is in the control regime the feedback amplitude is extremely small (see Fig. 5.24).

We should note that at the core of both the systems considered there is the same mechanism—the extension of the initial system's dimensions. In the first case, the dimensions increase due to the introduction of the external signal, and in the second one, due to the delay. The perturbation does not change the projection of the periodic orbit on the initial space of lower dimension. Additional degrees of freedom only change the Lyapunov exponents of the controlled system. We will explain this statement based on the example of the logistic mapping which we have already addressed many times. The unperturbed ($F_n = 0$) logistic mapping

$$X_{n+1} = 4X_n(1 - X_n) + F_n \tag{5.54}$$

has an unstable fixed point $X_n = 3/4$ with eigenvalue $\lambda = -2$. The perturbation in the delay form

$$F_n = K(X_{n-1} - X_n) \tag{5.55}$$

does not change the X coordinate of the fixed point, but increases the mapping dimension up to two. Analysis of that mapping shows that modules of the two eigenvalues of the Jacobi matrix for that point in the interval $K = [-1, -05]$ are less than unity. Therefore, for that value K the one-dimensional fixed point transforms into a two-dimensional stable point.

This scheme also suffers from the multi-stability problem related to the existence of two (or more) stable solutions with different basins of initial conditions. As in the case of control with external force, the multi-stability problem can be solved by introducing a limitation on the type (5.51) perturbation magnitude. Making use of this limitation, the asymptotic behavior of the system becomes single-valued for all K.

Figure 5.25 shows the dependence of the maximal Lyapunov exponent for period-1 ($\tau = 5.9$) and period-2 ($\tau = 11.75$) unstable orbits of the Rössler system. We can see that as in the case of the control with external force, each of the unstable orbits can be stabilized on the finite interval of K. However, those intervals are considerably narrower than in the former case. This means that the delayed control

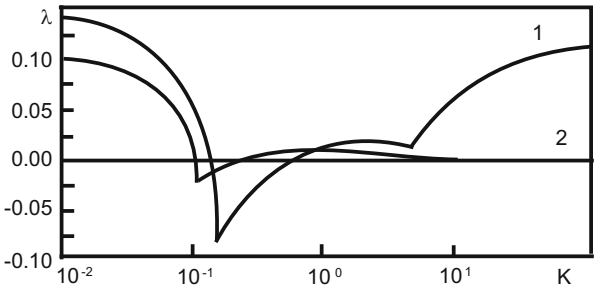

Fig. 5.25 Dependence of maximal Lyapunov exponent λ on K for period-1 ($\tau = 5.9$) and period-2 ($\tau = 11.75$) unstable orbits of the Rössler system in the case of continuous control with delayed feedback [44]

is more sensitive to the agreement of parameters, because the controlling external force always tries to attract the trajectory to the target periodic orbit. In the case of the control with delay, the perturbation brings the trajectory together with delayed one, which does not exactly coincide with the target orbit.

We now apply the continuous control scheme for stabilization of aperiodic (chaotic) orbits [46]. The considered scheme, using only a small perturbation of special form, allows us to synchronize the current behavior of the system with its past, previously recorded. As a result, we obtain the ability to predict long time segments of chaotic behavior. Essentially, the modern continuous control scheme is the combination of two different approaches to the chaos control problem: the OGY method, based on utilization for control of only a small perturbation with feedback, and the synchronization method (to be considered below) for two strongly connected chaotic systems. As the result of this synthesis we can synchronize aperiodic orbits due to a small perturbation with feedback.

As before, we assume that the controlled object is described by the system of the form (5.47) with all the above assumptions. The realization of the method splits into two stages. At the first stage, some time segment $y_{\text{ap}}(t)$ must be extracted and recorded. At the second stage, we apply to the system the feedback perturbation of the form

$$F(t) = K\left[y_{\text{ap}}(t) - y(t)\right] . \tag{5.56}$$

As well as above the perturbation represents a positive feedback, therefore $K > 0$. The block-diagram of experimental realization of the aperiodic orbits control method is presented in Fig. 5.26. One of the important features of the perturbation is the fact that it turns to zero when the output signal coincides with the one recorded in the system memory: $F(t) = 0$ for $y(t) = y_{\text{ap}}(t)$. Therefore, the perturbation

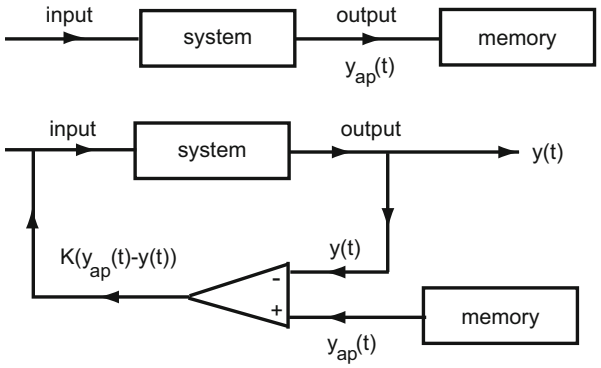

Fig. 5.26 Block-diagram of continuous control for aperiodic orbits

does not change the unperturbed system solution for the time interval corresponding to the recorded signal $y_{ap}(t)$. The perturbation, as in the case of unstable periodic orbits, works as the self-control because it always brings the current trajectory $y(t)$ to the target aperiodic orbit $y_{ap}(t)$. The synchronization can be achieved for a sufficiently large weight K. In the synchronization regime $\left(y_{ap}(t) \approx y(t)\right)$ the perturbation becomes very small (to the degree of $\left(y_{ap}(t) - y(t)\right)$ quantity).

The results of this synchronization for the Rössler, Lorenz, and Duffing systems are presented in Fig. 5.27. For all three systems, relatively soon after the perturbation turning on the current trajectory synchronizes with y_{ap}, i.e., $\Delta y \equiv y_{ap}(t) - y(t) \to 0$ relative to the degree of noise, and of the constancy of the system characteristics. Synchronization was achieved irrespective of the initial conditions (if they were chosen from a common basin).

The non-autonomous system, considered above as a control object and represented in Fig. 5.26, can be transformed into a more complex autonomous system containing two connected subsystems. Indeed, the memory unit used for the input signal generation in the first case, can be replaced by an additional identical chaotic system, which, starting from appropriate initial conditions, generates the aperiodic signal identical to the one recorded in memory.

As a result, the two-stage experiment is replaced by the single-stage one presented in Fig. 5.28. The original problem is therefore reduced to the synchronization of two connected identical chaotic systems, which will be considered later.

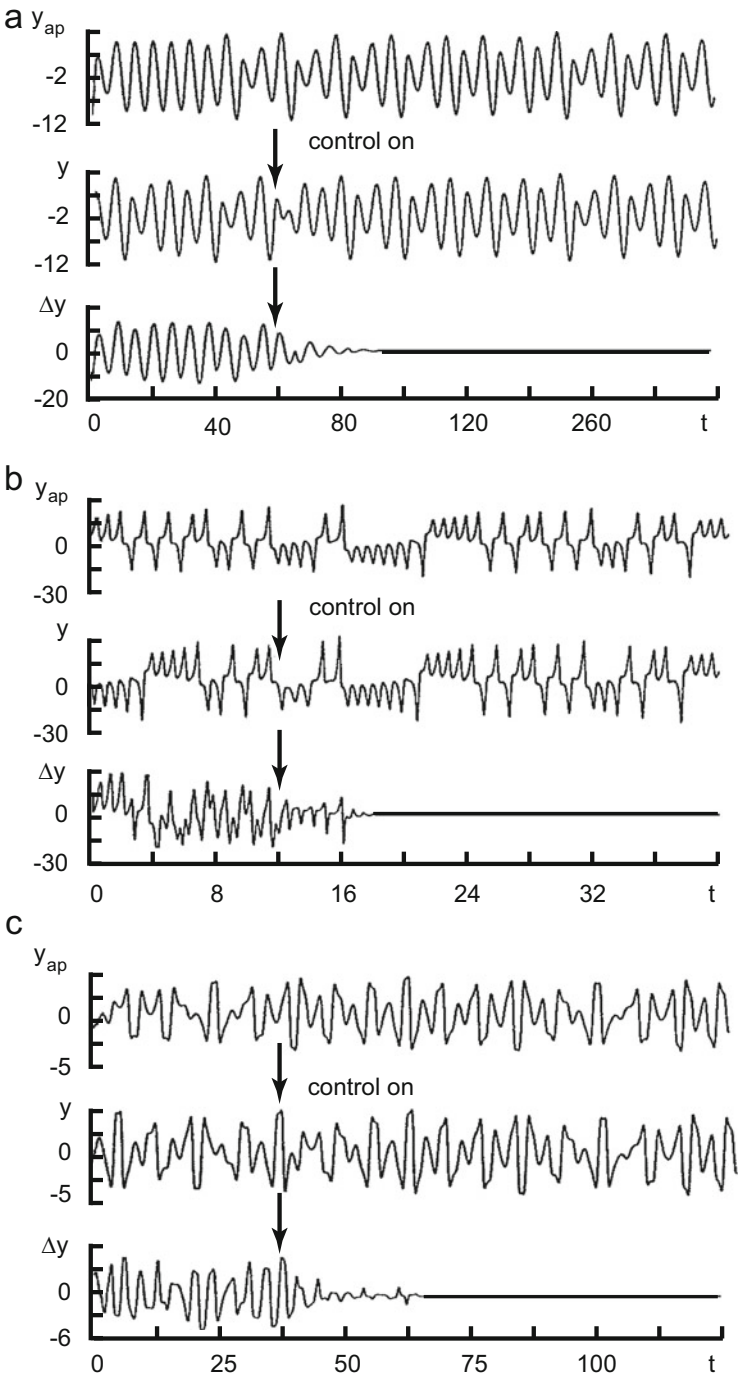

Fig. 5.27 Results of the aperiodic orbits control: (**a**) the Rössler system, (**b**) the Lorenz system, (**c**) the Duffing oscillator [46]

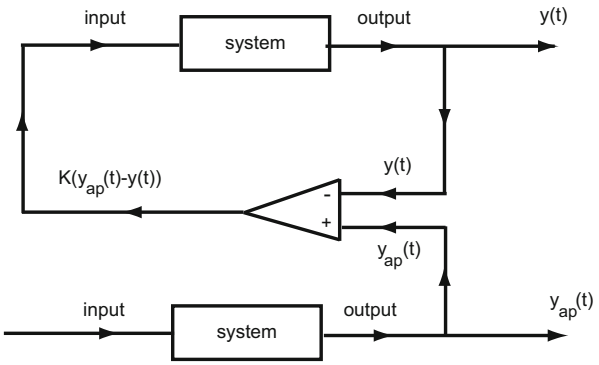

Fig. 5.28 Autonomous block-diagram for the aperiodic orbits control

References

1. Ott, E., Grebogi, C., Yorke, J.: Phys. Rev. Lett. **64**, 1196–1199 (1990)
2. Baker, G.: Am. J. Phys. **63**, 832–838 (1995)
3. Garfinkel, A., Spano, M.L., Ditto, W.L., Weiss, J.N.: Controlling Cardiac Chaos Sci. **257**, 1230–1235 (1992)
4. Schiff, S.J., Jerger, K., Duong, D.H., Chang, T., Spanno, M.L., Ditto, W.L.: Nature **370**, 615–620 (1994)
5. Berry, M.V.: Semiclassical Mechanics of Regular and Irregular Motion. Les Houches Lecture Series, vol. 36, pp. 171–270. North-Holland, Amsterdam (1983)
6. Gutzwiller, M.C.: Chaos in Classical and Quantum Mechanics. Springer, New York (1990)
7. Biham, O., Wenzel, W.: Phys. Rev. A **42**, 4639–4646 (1990)
8. Grassberger, P., Kantz, H., Moening, U.: J. Phys. A **22**, 5217–5230 (1989)
9. Hansen, K.: Phys. Rev. E **52**, 2388–2391 (1995)
10. Cvitanovic, P., Gunaratne, G.: Phys. Rev. A **38**, 1503–1520 (1988)
11. Schmelcher, P., Diakonos, F.: Phys. Rev. Lett. **78**, 4733–4736 (1997)
12. Boccaleti, S., Grebogi, C., Lai, Y.-C., Mancini, H., Maza, D.: Phys. Rep. **329**, 103–197 (2000)
13. Lai, Y.-C.: Comput. Phys. **8**, 62–67 (1994)
14. Feigenbaum, M.: J. Stat. Phys. **19**, 25–52 (1978)
15. Ditto, W., Spano, M.L., Linder, J.F.: Physica D **86**, 198–211 (1995)
16. Ditto, W.L., Showalter, K.: Chaos **7**, 509–511 (1997)
17. Hénon, M.: Commun. Math. Phys. **50**, 69–77 (1976)
18. Ott, E., Grebogi, C., Yorke, J.: In: Campbell, D.K. (ed.) Chaos: Soviet-American Perspectives on Nonlinear Science. American Institute of Physics, New York (1990)
19. Shinbrot, T., Grebogi, C., Ott, E., Jorke, J.A.: Nature **363**, 411–417 (1993)
20. Ditto, W.L., Rauseo, S.N., Spano, M.L.: Phys. Rev. Lett. **65**, 3211–3214 (1990)
21. Mandelbrot, B.: The Fractal Geometry of Nature. Freeman, San Francisco (1982)
22. Feder, J.: Fractals. Plenum Press, New York (1988)
23. Shinbrot, T., Ott, E., Grebogi, C., Jorke, J.A.: Phys. Rev. Lett. **65**, 3215–3218 (1990)
24. Shinbrot, T., Ditto, W., Grebogi, C., Ott, E., Spano, M., Yorke, J.A.: Phys. Rev. Lett. **68**, 2863–2866 (1992)
25. Kostelich, E., Grebogi, C., Ott, E., Jorke, J.A.: Phys. Rev. E **47**, 305–310 (1993)
26. Lai, Y.-C., Ding, M., Grebogi, C.: Phys. Rev. E **47**, 86–92 (1993)
27. Schroer, C., Ott, E.: Chaos **7**(4), 512–519 (1997)
28. Grebogi, C., Ott, E., Yorke, J.: Phys. Rev. Lett. **57**, 1284–1287 (1986)
29. Karney, C.: Physica D **8**, 360–380 (1983)

30. Lichtenberg, A.J., Lieberman, M.A.: Regular and Stochastic Motion. Springer, New York (1983)
31. Siegel, C.L., Mozer, J.: Lectures on Celestial Mechanics. Springer, Berlin (1971)
32. Bolt, E., Meiss, J.: Phys. Lett. A **204**, 373–378 (1995)
33. Lai, Y.-C., Tel, T., Grebogi, C.: Phys. Rev. E **48**, 709–717 (1993)
34. Gaspard, P., Rice, S.: J. Phys. Chem. **90**, 2225–2241 (1989)
35. Politi, A., Oppo, G.L., Badii, R.: Phys. Rev. A **33**, 486–490 (1986)
36. Gonchar, V.Yu., Ostapchyk, P.N., Tur, A.V., Yanovsky, V.V.: Phys. Lett. A **152**(5–6), 287–292 (1991)
37. Chirikov, B.V.: At. Energiya **6**, 630–638 (1959)
38. Bolotin, Yu.L., Gonchar, V.Yu., Tur, A.V., Yanovsky, V.V.: Phys. Rev. Lett. **82**, 2504–2507 (1999)
39. Poon, L., Grebogi, C.: Phys. Rev. Lett. **75**, 4023–4026 (1995)
40. Bolotin, Yu.L., Gonchar, V.Yu., Krokhin, A.A., Hernandes-Tejeda, P.H., Tur, A.V., Yanovsky, V.V.: Phys. Rev. E **64**, 0262XX1–0262XX9 (2001)
41. Ding, M., Ott, E., Grebogi, C.: Physica D **74**, 386–394 (1994)
42. Wiggins, S.: Introduction to Applied Nonlinear Dynamical Systems and Chaos. Springer, New York (1990)
43. Rössler, O.: Phys. Lett. A **57**, 397–398 (1976)
44. Pyragos, K.: Phys. Lett. A **170**, 421–428 (1992)
45. Lorenz, E.: J. Atmos. Sci. **20**, 130–141 (1963)
46. Pyragos, K.: Phys. Lett. A **181**, 203–210 (1993)